Progress in Neurobiology 202 (2021) 102033

Contents lists available at ScienceDirect

Progress in Neurobiology

journal homepage: www.elsevier.com/locate/pneurobio

Original Research Article

Causal role of cross-frequency coupling in distinct components of cognitive control

Justin Riddle [a,b], Amber McFerren [a,b], Flavio Frohlich [a,b,c,d,e,f,*]

[a] Department of Psychiatry, University of North Carolina at Chapel Hill, Chapel Hill, NC, 27599, USA
[b] Carolina Center for Neurostimulation, University of North Carolina at Chapel Hill, Chapel Hill, NC, 27599, USA
[c] Department of Neurology, University of North Carolina at Chapel Hill, Chapel Hill, NC, 27599, USA
[d] Department of Cell Biology and Physiology, University of North Carolina at Chapel Hill, Chapel Hill, NC, 27599, USA
[e] Department of Biomedical Engineering, University of North Carolina at Chapel Hill, Chapel Hill, NC, 27599, USA
[f] Neuroscience Center, University of North Carolina at Chapel Hill, Chapel Hill, NC, 27599, USA

ARTICLE INFO

Keywords:
Cross-frequency coupling
Cognitive control
Phase-amplitude coupling
EEG
Transcranial alternating current stimulation
Prefrontal cortex

ABSTRACT

Cognitive control is the capacity to guide motor and perceptual systems towards abstract goals. High-frequency neural oscillations related to motor activity in the beta band (13−30 Hz) and to visual processing in the gamma band (>30 Hz) are known to be modulated by cognitive control signals. One proposed mechanism for cognitive control is via cross-frequency coupling whereby low frequency network oscillations in prefrontal cortex (delta from 2−3 Hz and theta from 4−8 Hz) guide the expression of motor-related activity in action planning and guide perception-related activity in memory access. However, there is no causal evidence for cross-frequency coupling in these dissociable components of cognitive control. To address this important gap in knowledge, we delivered cross-frequency transcranial alternating current stimulation (CF-tACS) during performance of a task that manipulated cognitive control demands along two dimensions: the abstraction of the rules of the task (nested levels of action selection) that increased delta-beta coupling and the number of rules (set-size held in memory) that increased theta-gamma coupling. As hypothesized, we found that CF-tACS increased the targeted phase-amplitude coupling and modulated task performance of the associated cognitive control component. These findings provide causal evidence that prefrontal cortex orchestrates different components of cognitive control via two different cross-frequency coupling modalities.

1. Introduction

Thoughts and actions are guided towards internal goals via cognitive control (Braver, 2012; Norman and Shallice, 1986). The prefrontal cortex plays a primary role in cognitive control and provides feedback signals to motor (Koechlin et al., 2003) and perceptual (Gazzaley and Nobre, 2012) neural systems. For example, the rostral-caudal axis of the frontal cortex is organized hierarchically where the most caudal regions implement concrete motor actions and anterior regions are involved in motor planning, decision-making, and behavioral monitoring (Koechlin et al., 2003; Badre and Nee, 2018). With increased abstraction of task rules, the prefrontal cortex exerts greater top-down control over the motor cortex to guide action (Voytek et al., 2015a; Wyart et al., 2012; Picazio et al., 2014). In addition, the prefrontal cortex exerts top-down control over perceptual systems during memory and attention (Lee and D'Esposito, 2012; Kastner et al., 1999). In order for the prefrontal cortex to exert control over motor cortex and perceptual systems, network-level activity in the prefrontal cortex must modulate local activity in posterior cortex.

One candidate mechanism to support interregional communication is phase synchronization of neural oscillations (Fries, 2015). In this model, local high frequency neural activity typical of motor or perceptual cortices is modulated by low frequency neural oscillations typical of prefrontal cortex, which might be achieved via cross-frequency coupling (Canolty and Knight, 2010). One proposed mode of cross-frequency coupling is the control over motor-related beta oscillations that are modulated in the planning of action, execution of action, and post-action monitoring (Kilavik et al., 2013). Beta oscillations are proposed to inhibit activity in order to maintain a particular task-set (Buschman et al., 2012; Antzoulatos and Miller, 2016, 2014; Wutz et al., 2018a,

* Corresponding author at: 6108A Mary Ellen Jones Building, 116 Manning Drive, Chapel Hill, NC, 27599, USA.
E-mail address: flavio_frohlich@med.unc.edu (F. Frohlich).

https://doi.org/10.1016/j.pneurobio.2021.102033
Received 24 February 2021; Accepted 14 March 2021
Available online 16 March 2021

2018b; Wischnewski et al., 2020; Schmidt et al., 2019), and delta oscillations may reflect an update or switch in relevant rules (Antzoulatos and Miller, 2016; de Vries et al., 2018). Prefrontal control signals that orchestrate action are hypothesized to take the form of cross-frequency coupling between low-frequency delta oscillations in prefrontal cortex and beta oscillations in motor cortex (Wyart et al., 2012). Similarly, gamma oscillations in parietal-occipital cortex are modulated in the processing of visual information (Van Kerkoerle et al., 2014; Börgers and Kopell, 2008) as well as the encoding and retrieval of visual information (Jensen et al., 2007). Thus, prefrontal control signals to orchestrate perception and memory are hypothesized to take the form of coupling between theta oscillations in prefrontal cortex and gamma oscillations in parietal-occipital cortex (Berger et al., 2019). While there is emerging evidence for a causal role of cross-frequency coupling in cognitive control (Alekseichuk et al., 2016; Hermiller et al., 2020; Bramson et al., 2020; Berger et al., 2019; Turi et al., 2020; de Lara et al., 2018), there are only a few observational studies that investigate multiple motifs of cross-frequency coupling (Riddle et al., 2020; Voytek et al., 2010) and no study that investigated two distinct motifs of cross-frequency coupling in cognitive control.

Transcranial alternating current stimulation (tACS) is a non-invasive brain stimulation technique (Ali et al., 2013; Fröhlich, 2014) that can be used to deliver customizable waveforms that mimic endogenous phase-amplitude coupling activity patterns (Alekseichuk et al., 2016; Bramson et al., 2020; Turi et al., 2020; de Lara et al., 2018), and with a three-electrode montage two different brain regions can be synchronized (Polanía et al., 2012; Violante et al., 2017; Ahn et al., 2019). We recruited participants to perform a hierarchical cognitive control task that manipulated cognitive control demands along two dimensions: the level of abstraction of task rules and the number of rules (set-size) (Badre and D'Esposito, 2007; Riddle et al., 2020). In the initial baseline session, peak phase-amplitude coupling frequency pairs were localized from EEG and individualized waveforms designed to mimic this activity were used in subsequent sessions. In the remaining sessions, participants received cross-frequency tACS in either delta-nested beta, theta-nested gamma, or sham during performance of the hierarchical cognitive control task. We hypothesized that cross-frequency tACS would increase the targeted phase-amplitude coupling (quantified from inter-block resting-state periods after stimulation), delta-beta CF-tACS would modulate performance as a function of abstraction, and theta-gamma CF-tACS would modulate performance as a function of set-size.

2. Results

2.1. Two components of cognitive control

Twenty-seven participants were enrolled, and twenty-four participants completed, our four-session pre-registered experiment (National Clinical Trial 03800030). Two participants did not complete the experiment due to the time commitment and one participant decided to

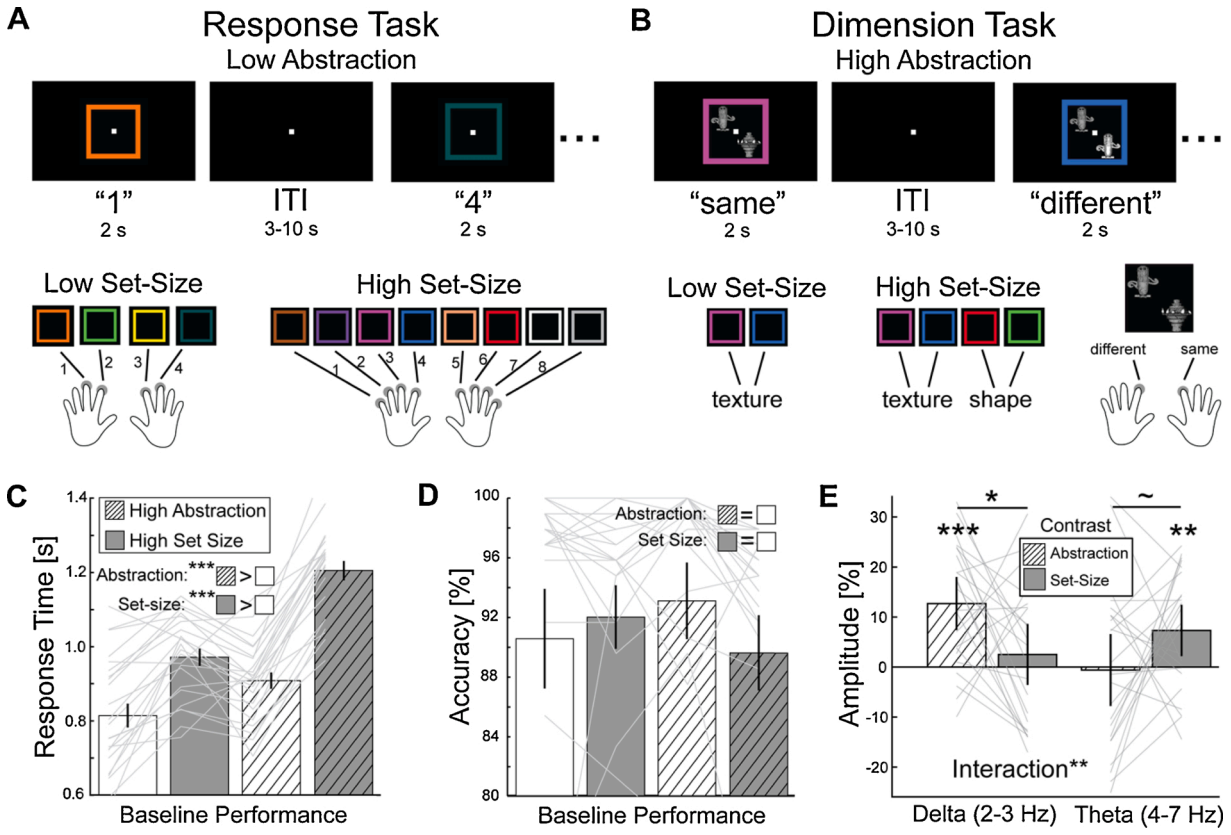

Fig. 1. *Hierarchical cognitive control paradigm.* (A) The response task consisted of a mapping between button response and colored square. This low abstraction task manipulated set-size with an increase in the number of color-to-button mapping from four to eight. (B) In the dimension task, two objects were presented within a colored square. The colored square mapped onto a feature dimension: texture or shape. The objects were evaluated based on this feature and were determined to be the "same" or "different." This high abstraction task manipulated set-size with an increase in the number of dimensions that were indicated by the colors, one or two. ITI is inter-trial interval. s is seconds. (C-D) Baseline behavioral performance was evaluated with a two-way repeated-measures ANOVA with factors: abstraction (high or low) and set-size (high or low). (C) Response time was slower as a function of abstraction (striped versus not-striped bars) and set-size (grey versus white bars). (D) For accuracy, there was no significant difference as a function of set-size or abstraction. (E) Repeated-measured ANOVA of the amplitude of low-frequency neural oscillations with two factors, band (delta or theta) and cognitive control component (abstraction or set-size), revealed a significant interaction. Time window for analysis: 0.2 to 1.6 s after stimulus. Activity was extracted from prefrontal electrodes (Fz and surrounding). Error bars are SEM. Opaque lines are individual traces. *** $p < 0.001$, ** $p < 0.01$, * $p < 0.05$, ~ $p < 0.1$, = $p > 0.1$.

discontinue participation. Another participant performed at chance for all stimulation conditions and was removed from analysis, resulting in 23 participants for the final analyses. While it is theoretically possible that the chance performance of the participant was due to stimulation, this is unlikely as performance was at chance even for sham stimulation, which suggested that the participant was not cognitively engaged for these sessions. Participants performed tasks within a hierarchical cognitive control paradigm that manipulated cognitive control demands along two dimensions: the abstraction of the rules and the set-size of the rules. The response task, low abstraction, involved the presentation of a colored square with a memorized association to a specific button on a keyboard (Fig. 1A). The number of color-to-button mappings that were maintained was the set-size, and was increased from four to eight. The dimensions task, high abstraction, involved the presentation of a colored square with two objects within it (Fig. 1B). The colored square mapped to a specific feature dimension, either texture or shape. The objects were evaluated based on the indicated feature dimension and a same or different judgement was made. The number of feature dimensions that were maintained was the set-size, and was increased from one to two. The set-size for each task was selected such that behavioral performance was comparable between abstraction levels. Analysis of baseline performance by two-way repeated-measures ANOVA revealed that response time was slower as a function of task abstraction (average difference 164 ± 101 ms, $F(1,22) = 60.12$, $p = 9.88e\text{-}08$, $\eta_p^2 = 0.73$), and of set-size (average difference 227 ± 84 ms, $F(1,22) = 166.6$, $p = 9.69e\text{-}12$, $\eta_p^2 = 0.88$) (Fig. 1C). In addition, the interaction between abstraction and set-size was significant ($F(1,22) = 24.56$, $p = 5.86e\text{-}05$, $\eta_p^2 = 0.53$) and driven by a marked increase in reaction time for the high abstraction and high set-size condition relative to all others (average difference 307 ± 105 ms). Analysis of accuracy revealed an interaction between abstraction and set-size ($F(1,22) = 4.38$, $p = .048$, $\eta_p^2 = 0.17$) partially driven by a decrease in accuracy for the high abstraction and high set-size condition relative to all others (average difference -2.28 ± 4.61 %, $t(22) = -2.37$, $p = 0.027$, $d = 0.49$), but no main effect of abstraction (average difference 0.07 ± 4.97 %, $F(1,22) = 0.01$, $p = .95$, $\eta_p^2 = 0.00$) or set-size (average difference -1.02 ± 4.46 %, $F(1,22) = 1.23$, $p = .28$, $\eta_p^2 = 0.05$) in the baseline session (Fig. 1D). These findings provide evidence that behavioral performance was influenced by task demands along both components of cognitive control.

2.2. Low-frequency oscillations in prefrontal electrodes

From our previous experiment (Riddle et al., 2020), we expected to replicate an interaction between low-frequency band (delta or theta) and cognitive control component (abstraction or set-size) on the amplitude of low-frequency oscillatory activity in prefrontal electrodes (Fz and surrounding). Two-way repeated-measures ANOVA revealed the hypothesized significant interaction ($F(1,22) = 10.13$, $p = 0.0043$, $\eta_p^2 = 0.32$) (Fig. 1E), and no main effect of cognitive control component ($F(1, 22) = 0.12$, $p = 0.73$, $\eta_p^2 = 0.005$) or low-frequency band ($F(1,22) = 2.517$, $p = 0.13$, $\eta_p^2 = 0.10$). Post-hoc tests revealed a significant increase in delta oscillations for abstraction greater than set-size ($t(22) = 2.48$, $p = 0.025$, $d = 0.52$), and a trend-level increase in theta oscillations for set-size greater than abstraction ($t(22) = 1.75$, $p = 0.093$, $d = 0.37$). Time-frequency analysis revealed a significant decrease in alpha-beta oscillations (8−30 Hz) from 0.4 s to 1.5 s after stimulus onset as a function of abstraction (Fig. 2A) and set-size (Fig. 2B). The decrease in beta oscillations for both contrasts survived permutation-based cluster

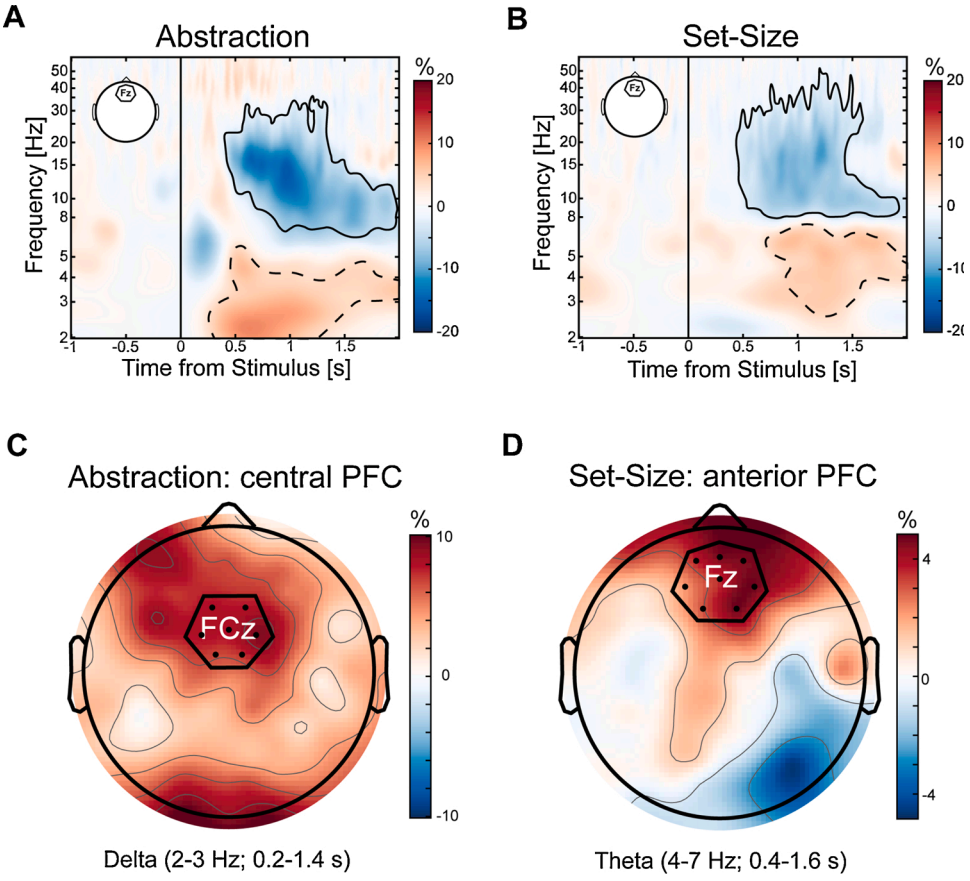

Fig. 2. *Time-frequency analysis of cognitive control components.* Five-cycle Morlet wavelet convolution was run on prefrontal electrodes (Fz and surrounding). (A) As a function of abstraction, statistical analysis revealed a decrease in alpha-beta oscillations (6-30 Hz) from 0.3 to 1.6 s following the stimulus and an increase in delta oscillations (2-4 Hz) from 0.2 to 1.4 s. (B) As a function of set-size, statistical analysis revealed a decrease in alpha-beta oscillations (8-30 Hz) from 0.4 to 1.4 s following the stimulus and an increase in theta oscillations (3-8 Hz) from 0.6 to 1.6 s. Units are percent change from baseline (-0.6 to -0.3 s) for all panels. Graphic in the upper right corner depicts the region of interest used for time-frequency analysis. Frequencies on the y-axis are log-scale using a $1/f^{0.05}$ distribution. Zero point is the time that the stimulus was presented. Solid line depicts time-frequency clusters that survived permutation-based cluster-mass correction at $p < 0.05$. Dashed line depicts time-frequency clusters that were significant at $p < 0.05$, $k > 1000$. (C) Topographic distribution of the amplitude of delta band as a function of abstraction shows a peak near the frontal-central midline. FCz and surrounding electrodes from 0.2 to 1.4 s was defined as central prefrontal cortex for delta-beta PAC analysis. (D) Topographic distribution of the amplitude of theta band as a function of set-size shows a peak near the frontal midline. Fz and surrounding electrodes from 0.4 to 1.6 s was defined as anterior prefrontal cortex for theta-gamma PAC analysis. Outlined polygon depicts the electrodes defined for each region of interest and black dots are the electrodes. The central electrode is written in white.

correction. In addition, we found an increase in delta oscillations (peak from 2−3 Hz, and 0.2–1.4 seconds) with abstraction (Fig. 2A) and theta oscillations (peak from 2−3 Hz, and 0.6–1.6 seconds) with set-size (Fig. 2B) at $p < 0.05$ and $k > 1000$, but these clusters did not survive permutation-based cluster correction. Time-frequency analysis was used to localize the low-frequency seed region and time window for phase-amplitude coupling analysis. Based on the topographic plot of delta-oscillations as a function of abstraction, the central prefrontal cortex (FCz and its surrounding electrodes) was selected for phase-amplitude coupling analysis (Fig. 2C). Based on the topographic plot of theta-oscillations as a function of set-size, the anterior prefrontal cortex (Fz and its surrounding electrodes) was selected (Fig. 2D). Region of interest localization ensured the presence of low frequency oscillations in prefrontal electrodes such that the phase of task-evoked oscillations was interpretable.

2.3. Distinct cross-frequency coupling by cognitive control component

Cross-frequency coupling analysis was run between the phase of low frequency oscillations in prefrontal electrodes with the amplitude of high frequency activity across the scalp. Delta-beta coupling was hypothesized to increase as a function of abstraction and theta-gamma as a function of set-size. Using the central prefrontal regions of interest derived from time-frequency analysis, phase-amplitude coupling analysis revealed an increase in delta-beta coupling with the right motor cortex and anterior frontal electrodes (Fig. 3A). Canonical motor electrode C4 and five of its six surrounding electrodes (rM1) displayed a significant increase in delta-beta coupling as a function of abstraction. This coupling pattern suggests that delta oscillations provide top-down control over motor-related beta activity as abstraction is increased. In addition, the phase of theta oscillations in prefrontal electrodes was hypothesized to be coupled to the amplitude of gamma oscillations in parietal-occipital electrodes and theta-gamma coupling was hypothesized to be increased as a function of task set-size. Using the anterior prefrontal regions of interest derived from time-frequency analysis, phase-amplitude coupling analysis indeed revealed an increase in coupling with the bilateral parietal-occipital electrodes (Fig. 3B). Electrodes between Pz and the central midline (ParOcc) displayed a significant increase in theta-gamma coupling by set-size. Together, these findings support a model where delta and theta oscillations in prefrontal

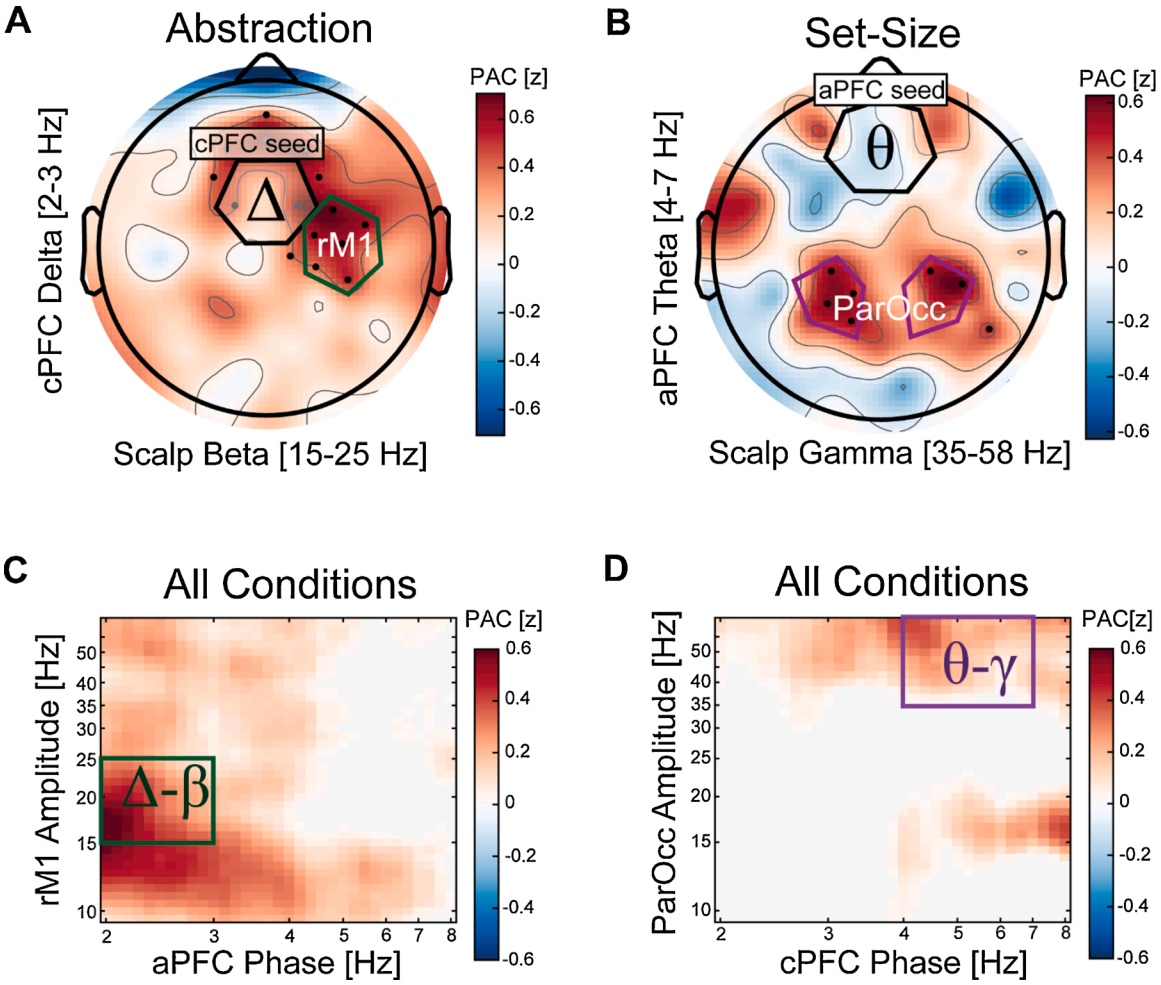

Fig. 3. *Phase-amplitude coupling during hierarchical cognitive control.* (A) The phase of delta oscillations (2-3 Hz) in central prefrontal electrodes (cPFC) to the amplitude of beta oscillations (15-25 Hz) across the scalp as a function of abstraction revealed a significant increase in coupling over frontal-midline and right motor electrodes (rM1), and (B) theta phase (4-7 Hz) in anterior prefrontal electrodes (aPFC) to gamma amplitude (35-58 Hz) as a function of set-size revealed a significant increase in coupling in parietal-occipital electrodes (ParOcc). cPFC and aPFC regions of interest are highlighted with a black hexagon and marked with a Greek letter referring to the canonical frequency band. Black dots depict electrodes with a significant increase in coupling for high versus low abstraction/set-size ($p < 0.05$). Motor electrodes are highlighted in green with the central electrode, C4 and labeled as rM1 in white. ParOcc is outlined in purple. (C-D) Endogenous phase-amplitude coupling was investigated across all conditions to check for frequency-specificity of coupling. Across all task conditions, the average coupling strength between phase of low-frequency oscillations (2-8 Hz) and high-frequency oscillations (9-58 Hz) from (C) cPFC to rM1 and (D) aPFC to bilateral ParOcc. Highlighted region in green/purple depicts the range used for delta-beta/theta-gamma coupling analysis.

cortex guide action-planning and memory-dependent task-set maintenance, respectively.

To investigate whether the coupling patterns that increased as a function of abstraction and set-size represented the primary coupling mode, an exhaustive comodulogram of coupling strength for all task conditions between low-frequency phase (2−8 Hz) and high-frequency amplitude (9−58 Hz) was run. From cPFC to rM1 (C4 and surrounding electrodes), peak coupling strength was found in the frequency pair: 2.0–15.9 Hz and ranged from 2−4 Hz and 10−25 Hz (Fig. 3C). This analysis suggests that delta-beta coupling from prefrontal to motor cortex was frequency-specific and upregulated by increasingly abstract rules. From aPFC to ParOcc (bilateral cluster between Pz and the central midline), peak coupling was found in the frequency pair: 4.1–58 Hz and extended from 3 to 8 Hz and 40–58 Hz (Fig. 3D). Similarly, this analysis suggests that theta-gamma coupling from prefrontal to parietal-occipital cortex is frequency-specific and upregulated as a function of set-size. These coupled regions of interest derived at baseline were used to quantify the efficacy of CF-tACS to modulate phase-amplitude coupling.

2.4. Causal investigation of phase-amplitude coupling in cognitive control

Causal evidence is required to substantiate correlational findings. Transcranial alternating current stimulation (tACS) allows for the delivery of custom electrical waveforms that mimic endogenous activity patterns (Fröhlich and McCormick, 2010). Here, the stimulation waveform was designed to mimic the phase-amplitude coupling relationship between prefrontal electrodes and posterior electrodes (see (Alekseichuk et al., 2016) for a similar method). By individualizing the stimulation waveform to each participant, the efficacy of stimulation is enhanced as neural entrainment is achievable with minimal stimulation amplitude, i.e. the Arnold tongue (Ali et al., 2013; Negahbani et al., 2018). Thus, baseline EEG activity was used to customize the waveform of cross-frequency tACS (CF-tACS). Local phase-amplitude coupling between central prefrontal electrodes (FCz and surrounding) was used to localize the frequency pair with peak delta-beta coupling (phase of 2−4 Hz and amplitude of 15−30 Hz) in the high abstraction, high set-size condition (Fig. 4A) and peak theta-gamma coupling (phase of 4−8 Hz and amplitude 35−59 Hz) in the low abstraction, high set-size condition (Fig. 4B). Each waveform comprised a low-frequency component with a high-frequency component nested at the peak of the low-frequency waveform (Table 1).

For the second, third, and fourth sessions, participants received CF-tACS in delta-beta frequency, theta-gamma frequency, or sham (placebo) in a randomized and counter-balanced order (Fig. 4C). CF-tACS was delivered during performance of the hierarchical cognitive control task. Resting-state periods were included after each task block, as CF-tACS was hypothesized to increase the targeted phase-amplitude coupling, but the EEG was corrupted during stimulation so the aftereffects of stimulation during rest were instead quantified. A three-

Table 1
Descriptive statistics of individualized stimulation frequencies.

Hertz	Delta (Δ)	Beta (β)	Theta (θ)	Gamma (γ)	Diff(θ, Δ)	Diff(β, γ)
Range (min)	2.00	18.00	5.00	39.00	2.00	14.25
Range (max)	4.00	27.75	7.50	59.00	5.50	37.00
Mean	2.63	22.20	6.31	49.95	3.69	27.75
Standard deviation	0.64	2.32	0.79	6.07	1.07	6.42

Cross-frequency pair used for stimulation was individualized based on phase-amplitude coupling at baseline. The descriptive statistics (range, mean, and standard deviation) for each frequency band (rows 2–5) are included here. In addition, descriptive statistics for the difference in frequency between low frequencies (theta and delta) and high frequencies (gamma and beta) is included. The unit for all values is Hertz. Diff(X,Y) refers to the within-participant difference of X from Y. N = 23.

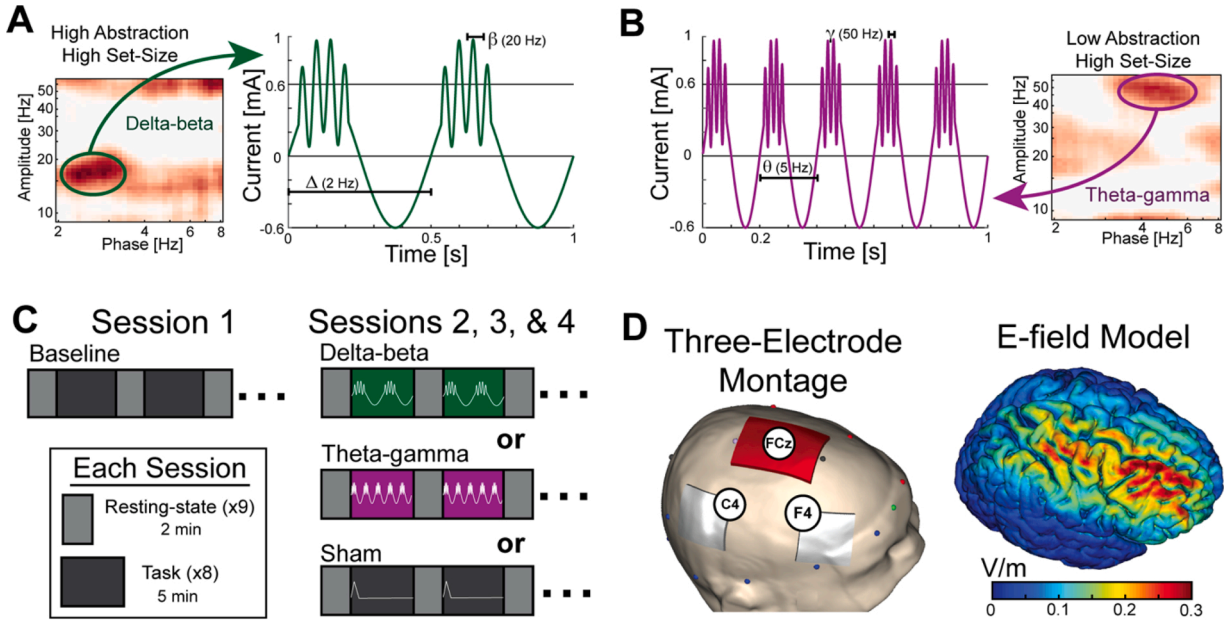

Fig. 4. *Causal Investigation using Cross-Frequency Transcranial Alternating Current Stimulation*. Cross-frequency transcranial alternating current stimulation (CF-tACS) was delivered using individualized waveforms designed to mimic and enhance endogenous delta-beta and theta-gamma phase-amplitude coupling. (A) Peak phase-amplitude coupling for delta-beta was extracted from the high abstraction, high set-size condition at baseline, and was used to generate a custom electric waveform. (B) Peak theta-gamma coupling was extracted from the low abstraction, high set-size condition. (C) In a crossover design, participants received CF-tACS during performance of the cognitive control tasks. Resting-state periods without stimulation were included after each task block to quantify the effect of CF-tACS on neural activity. Delta-beta CF-tACS in green, theta-gamma CF-tACS in purple, and sham in dark grey. (D) A three-electrode montage was used with two stimulation devices, in order to deliver identical current to the prefrontal (anterior to F4) and the motor cortex (posterior to C4). The return electrode centered on the central midline, FCz. CF-tACS was targeted to increase coupling between right lateral prefrontal cortex and right posterior cortex via in-phase stimulation. Peak electric field was calculated to be along the right middle frontal gyrus and the hand region of the right motor cortex. Units are volts per meter.

electrode montage was used such that the two target electrodes would receive in-phase synchronized stimulation (Polanía et al., 2012; Violante et al., 2017; Ahn et al., 2019). The anterior electrode (4.5 by 4.5 cm) was placed anterior and ventral to the F4 position and the posterior electrode (4.5 by 4.5 cm) was placed posterior and ventral to the C4 position (Fig. 4D). The return electrode (5 by 7 cm) was centered posterior to anterior over the FCz position. The montage was selected such that the resulting electric field was centered on the rostral-caudal axis of the right middle frontal gyrus which is implicated in hierarchical cognitive control (Badre and D'Esposito, 2007) (Fig. 4E). CF-tACS was hypothesized to increase phase-amplitude coupling within the targeted frequency-pairs.

2.5. Causal evidence for phase-amplitude coupling in components of cognitive control

To investigate whether cross-frequency coupling plays a causal role in cognitive control and is not epiphenomenal, CF-tACS was delivered in a frequency-specific manner during task performance to modulate distinct cognitive control processes. Delta-beta CF-tACS was hypothesized to modulate behavior as a function of abstraction and theta-gamma CF-tACS to modulate behavior as a function of set-size. We investigated accuracy and reaction time using three-way repeated-measures ANCOVA with factors frequency of CF-tACS (delta-beta CF-tACS, theta-gamma CF-tACS, or sham) and components of hierarchical cognitive control, abstraction (high or low) and set-size (high or low). In addition, a linear factor for sequence was included. For reaction time, we found a significant interaction between stimulation and abstraction ($F(2,21) = 4.253$, $p = .0281$, $\eta^2_p = .288$) (Table 2) that was driven by an increase in reaction time for the abstraction contrast that was significant for delta-beta CF-tACS versus sham ($t(22) = 2.305$, $p = 0.031$, $d = .48$) (Fig. 5A). There was no interaction between stimulation and set-size for reaction time ($F(2,21) = 0.532$, $p = .595$, $\eta^2_p = .030$). For accuracy, we found a significant interaction between stimulation and set-size ($F(2,21) = 4.98$, $p = .017$, $\eta^2_p = .322$) (Table 3) that was driven by an increase in accuracy for the set-size contrast that was significant for theta-gamma CF-tACS versus sham ($t(22) = 2.989$, $p = .007$, $d = .623$) (Fig. 5B). There was no interaction between stimulation and abstraction for accuracy ($F(2,21) = 0.145$, $p = .866$, $\eta^2_p = .014$). All stimulation conditions are displayed in Fig. S1. Contrary to our hypothesis that stimulation would improve performance, delta-beta CF-tACS increased reaction time, albeit specifically to the targeted cognitive control dimension. Together, these findings provide causal evidence for delta-beta coupling in abstraction and theta-gamma coupling in set-size. The double dissociation of cross-frequency coupling in different components of cognitive control suggests a similar mechanism for control processes using distinct frequency bands.

Table 2
Repeated-measures analysis of covariance (RM-ANCOVA) for reaction time.

RM-ANCOVA 3-Way	Df	F-statistic	p-value	η^2_p
Stim	2, 21	0.09	0.915	0.008
Stim X Abs	**2, 21**	**4.253**	**0.0281***	**0.288**
Stim x Set	2, 21	0.532	0.595	0.030
Stim X Abs X Set	2, 21	0.34	0.716	0.031

Main effect and interactions with stimulation are reported here. Significance presented here was quantified using type 1 sum of squares with random effects of stimulation, after modeling random effects of the stimulation sequence. Input to "aov" in the "sjstats" toolbox in R: $RT = stim * abs * set + Error(\frac{subject}{session * stim * abs * set})$. RT refers to the response time of the task condition. Stim refers to the three stimulation conditions: delta-beta CF-tACS, theta-gamma CF-tACS, or sham. Abs refers to the level of abstraction of the task condition (high or low). Set refers to the level of set-size of the task condition (high or low). Error is the modeled random effects grouped by subject. * $p < .05$ in bold. $N = 23$.

2.6. Frequency-specific enhancement of phase-amplitude coupling by cross-frequency tACS

Eyes-open resting-state EEG was collected for 2 min immediately following each task block to analyze the immediate aftereffects of stimulation on phase-amplitude coupling. The post-stimulation resting-state periods were concatenated and phase-amplitude coupling (PAC) was calculated for the localized regions of interest: cPFC to rM1 for delta-beta coupling and aPFC to ParOcc for theta-gamma coupling. PAC was hypothesized to increase in the targeted frequency pair when stimulation was delivered in the same cross-frequency pair greater than stimulation in the other cross-frequency pair. The difference in phase-amplitude coupling from sham was submitted to an a priori interaction analysis with the hypothesis that delta-beta CF-tACS increased delta-beta PAC from cPFC to rM1 and theta-gamma CF-tACS increased theta-gamma PAC from aPFC to ParOcc relative to the other frequency of stimulation (Fig. 5C). In line with our hypothesis, we found a significant interaction between the cross-frequency of stimulation and cross-frequency of PAC (one-tail, $t(22) = 1.806$, $p = 0.042$, $d = 0.38$). Post-hoc tests show a numerically consistent, but not significant, increase in delta-beta PAC from delta-beta CF-tACS relative theta-gamma CF-tACS (one-tail, $t(22) = 0.707$, $p = 0.243$, $d = 0.147$) and a trend-level increase in theta-gamma PAC from theta-gamma CF-tACS relative to delta-beta CF-tACS (one-tail, $t(22) = 1.664$, $p = 0.055$, $d = 0.347$). To control for any sequence effects, a three-way repeated-measures ANCOVA was run that investigated the hypothesized interaction between stimulation (delta-beta, theta-gamma, or sham) and PAC strength (delta-beta, theta-gamma) with session number as a linear control factor (interaction: $F(2,21) = 3.148$, $p = 0.063$, $\eta^2_p = 0.231$) (Table 4). Finally, there was no difference between delta-beta PAC and theta-gamma PAC for sham stimulation ($t(22) = -0.470$, $p = .643$, $d = .098$). Thus, CF-tACS successfully enhanced the phase-amplitude coupling pattern that was observed during the hierarchical cognitive control task in a frequency-specific manner.

CF-tACS may have increased phase-amplitude coupling in other regions that were not hypothesized. As an exploratory analysis, the impact of CF-tACS across the scalp was investigated. This analysis revealed that with a delta-phase seed in cPFC there was a significant increase in delta-beta coupling with a cluster of electrodes in the left midline overlapping with left motor electrodes (Fig. 6A). There was no significant increase in delta-beta coupling with theta-gamma tACS (Fig. 6B). Given the unexpected decrease in performance as a function of abstraction with delta-beta tACS, the impact of delta-beta tACS on phase-amplitude coupling was also unexpected. Recruitment of coupling with the homologous motor cortex from stimulation suggests that the network was reconfigured. With a theta-phase seed in aPFC, there was no significant increase in theta-gamma coupling from delta-beta tACS (Fig. 6C), but there was an increase in theta-gamma coupling in right parietal-occipital electrodes (Fig. 6D). The increase in theta-gamma PAC from theta-gamma tACS aligns with the targeted regions in the right hemisphere.

The topographic analysis of phase-amplitude coupling revealed a reconfiguration of interregional PAC from prefrontal electrodes to right motor electrodes at baseline to left motor electrodes after delta-beta tACS. To investigate the exploratory hypothesis that the motor-control network was reconfigured, we analyzed whether CF-tACS increased low-frequency functional connectivity within the network (see (Alekseichuk et al., 2016) for a similar analysis). Thus, we dropped a delta-frequency seed in the left motor cortex (C3) and investigated whether there was an increase in functional connectivity to the motor-control network (cPFC and rM1 regions of interest). In support of this post-hoc analysis, we found a significant increase in functional connectivity to the motor control network for delta-beta tACS relative to sham (mean 0.031, std = 0.048, $t(22) = 3.07$, $p = 0.00558$). Topographic analysis revealed that the increase in delta-frequency functional connectivity was spatially specific to the motor control network (Fig. 7A). As a control analysis, we did not find a significant increase in

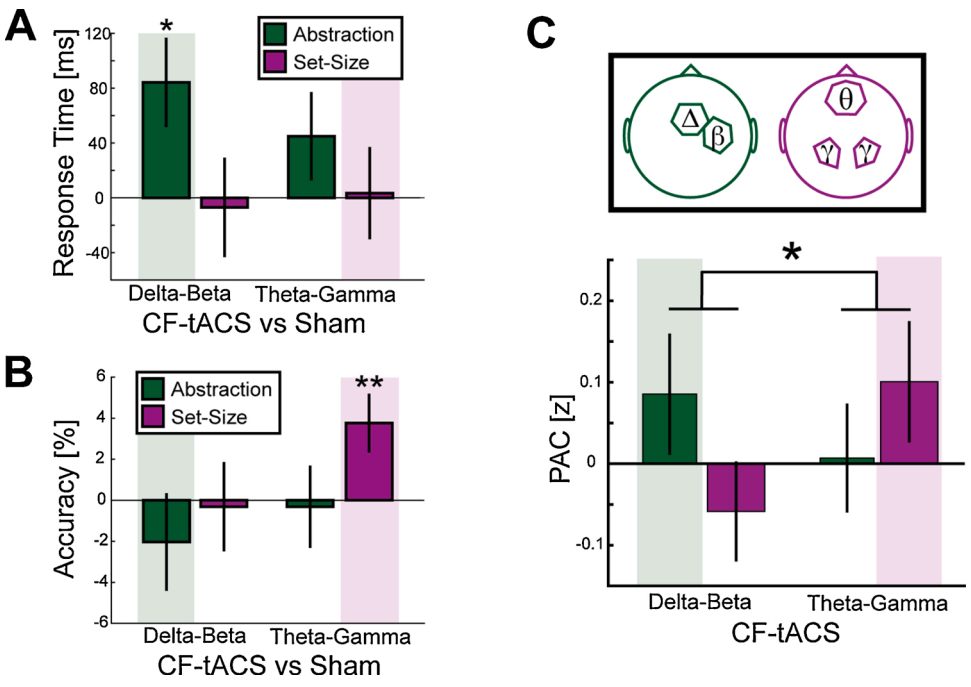

Fig. 5. *Impact of CF-tACS on behavior and phase-amplitude coupling.* (A-B) The impact of CF-tACS on behavioral performance was investigated as a function of different components of cognitive control (abstraction in green and set-size in purple). (A) Delta-beta CF-tACS increased response time only as a function of abstraction. (B) Theta-gamma CF-tACS increased accuracy only as a function of set-size. Opaque colored background depicts the condition for which an effect of stimulation was expected. * $p < .05$, ** $p < .01$. Error bars are SEM. (C) CF-tACS in either delta-beta or theta-gamma frequency was hypothesized to enhance the phase-amplitude coupling pattern that was present at baseline: coupling of the phase of delta oscillations in central prefrontal electrodes (cPFC) to the amplitude of beta oscillations in right motor electrodes (rM1) (green) and coupling of the phase of theta oscillations in anterior prefrontal electrodes (aPFC) to the amplitude of gamma oscillations in parietal-occipital electrodes (ParOcc) (purple). Hypothesized increase is highlighted by a colored background. The hypothesized interaction of frequency pair of stimulation by frequency-specific coupling strength was significant (one-tail, * $p < 0.05$). PAC is phase-amplitude coupling.

Table 3
Repeated-measures analysis of covariance (RM-ANCOVA) for accuracy.

RM-ANCOVA 3-Way	Df	F-statistic	p-value	η_p^2
Stim	2, 21	2.607	0.097~	0.199
Stim X Abs	2, 21	0.145	0.866	0.014
Stim x Set	**2, 21**	**4.98**	**0.017***	**0.322**
Stim X Abs X Set	2, 21	0.671	0.522	0.100

Main effect and interactions with stimulation are reported here. Significance presented here was quantified using type 1 sum of squares with random effects of stimulation, after modeling random effects of the stimulation sequence. Input to "aov" in the "sjstats" toolbox in R: $Acc = stim * abs * set + Error(\frac{subject}{session * stim * abs * set})$. Acc refers to the accuracy of the task condition. Stim refers to the three stimulation conditions: delta-beta CF-tACS, theta-gamma CF-tACS, or sham. Abs refers to the level of abstraction of the task condition (high or low). Set refers to the level of set-size of the task condition (high or low). Error is the modeled random effects grouped by subject. * $p < .05$ in bold. ~ $p < .10$. N = 23.

Table 4
Repeated-measures analysis of covariance (RM-ANCOVA) for phase-amplitude coupling (PAC).

RM-ANCOVA 2-Way	Df	F-statistic	p-value	η_p^2
Endo	1, 22	0.002	0.963	0.000
Stim	2, 21	1.976	0.164	0.158
Stim X Endo	**2, 21**	**3.148**	**0.0637~**	**0.231**

An interaction was hypothesized between the frequency of stimulation and the targeted endogenous activity. Endo refers to the endogenous activity that was measured: delta-beta coupling between cPFC and rM1 or theta-gamma coupling between aPFC and ParOcc. Accounting for random effects of session, ANCOVA using type 1 sum of squares revealed a trend-level interaction between the targeted phase-amplitude coupling (endo) and the frequency of stimulation (stim). Input to "aov" in the "sjstats" toolbox in R: $PAC = stim * endo + Error(\frac{subject}{session * stim * endo})$. Stim refers to the three stimulation conditions: delta-beta CF-tACS, theta-gamma CF-tACS, or sham. Session refers to the sequence of sessions (1, 2, or 3) modeled for a linear effect of time. Error is the modeled random effects grouped by subject. ~ $p < .10$ in bold.

delta-frequency functional connectivity with the motor-control network for theta-gamma tACS relative to sham (mean = 0.007, std = 0.041, t (22) = 0.834, p = 0.413) (Fig. 7B). Consistent with network reconfiguration, delta-beta tACS increased functional connectivity within the motor-control network.

3. Discussion

High frequency oscillations are increased during local information processing related to action (beta) and perception (gamma). The prefrontal cortex provides top-down control signals via cross-frequency coupling with high frequency activity in posterior cortex. We found that delta oscillations in central prefrontal electrodes coupled to beta oscillations in motor electrodes as a function of the abstraction of the rules. In addition, theta oscillations in anterior prefrontal electrodes coupled to gamma oscillations in parietal-occipital electrodes as a function of set-size, or the number of rules. We investigated the causal role of phase-amplitude coupling in cognitive control by delivering cross-frequency transcranial alternating current stimulation (CF-tACS) to enhance task-driven coupling relationships. After individualizing stimulation to peak cross-frequency coupling in each participant, we found that CF-tACS resulted in a frequency-specific increase in the targeted phase-amplitude coupling pattern. Furthermore, stimulation modulated task performance in the specific component of cognitive control that was targeted. Collectively, these findings demonstrate a rational approach (Kurmann et al., 2018): identification that phase-amplitude coupling increased with different components of cognitive control, stimulation designed to mimic this activity successfully engaged these signals, and validation of a causal role of cross-frequency coupling in distinct components of cognitive control based on frequency-specific modulation of behavior.

These findings contribute to a growing recognition of two distinct ranges of low frequency oscillations. Our time-frequency analysis found that delta oscillations (2−4 Hz) increased for one component of cognitive control associated with increased abstraction required for action selection and theta oscillations (4−8 Hz) increased for a different component of cognitive control associated with increased memory access. A recent experiment using nested rules, or direct-mapping rules, similar to the hierarchical cognitive control task reported here, found a

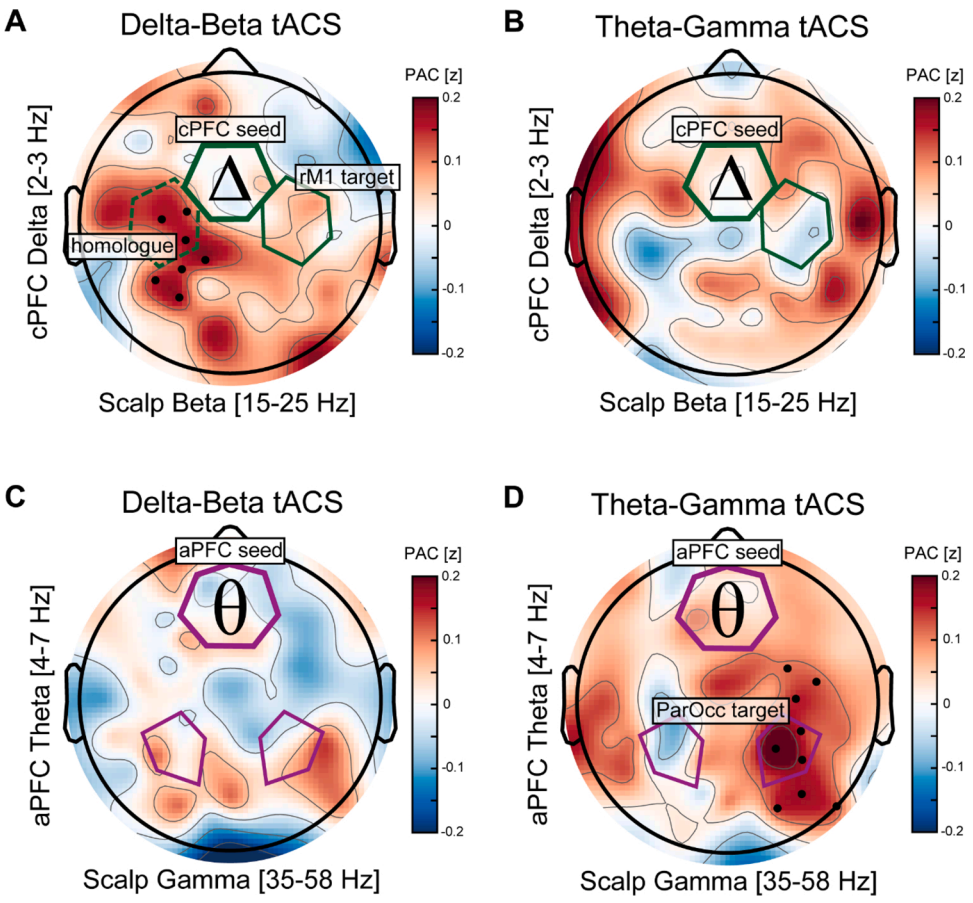

Fig. 6. *Topography of CF-tACS on phase-amplitude couplings*. (A) With a delta-phase seed in central prefrontal cortex (cPFC; green hexagon), there was an increase in coupling to beta-amplitude over left motor electrodes. The homologue to right motor electrodes (rM1) is indicated with a dashed green hexagon. (B) There was no increase in delta-beta coupling with theta-gamma tACS. (C) Delta-beta tACS did not have a significant impact on theta-gamma coupling. Theta-frequency phase in anterior prefrontal cortex (aPFC seed; purple heptagon) was investigated for coupling with gamma-frequency amplitude across the scalp. The theta-gamma coupled regions identified in baseline are outlined in purple. (D) With a theta-phase seed in aPFC, there was an increase in coupling to gamma-amplitude in right parietal-occipital electrodes. Parietal-occipital electrodes (ParOcc) identified in baseline analysis are outlined with purple pentagons. Black dots are $p < 0.05$ for electrode cluster with at least three contiguous electrodes.

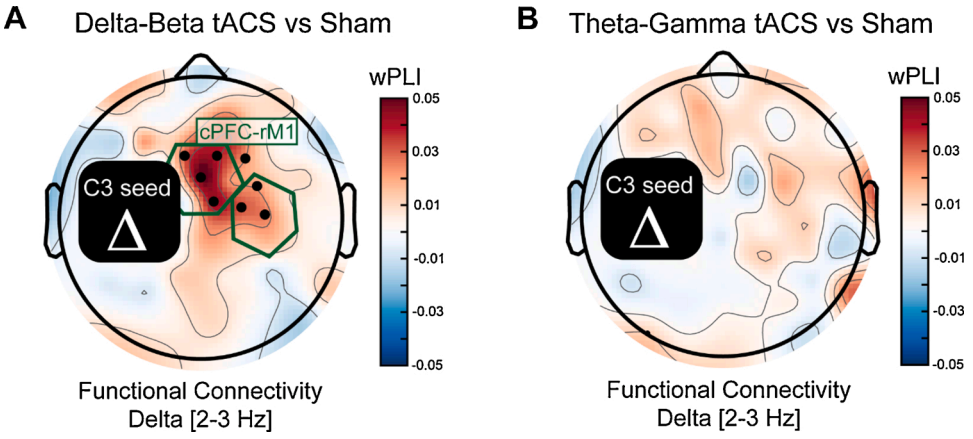

Fig. 7. *Low-frequency functional connectivity analysis*. (A) Investigation of delta frequency (2-3 Hz) functional connectivity between a seed in a left motor electrode (C3) revealed an increase in connectivity strength for delta-beta tACS relative to sham. (B) For theta-gamma tACS versus sham, there was no change in delta-frequency functional connectivity with the left motor region. Black rectangle shows the region excluded from analysis due to artifacts arising from local connectivity estimates. Black dots represent electrodes with a significant effect at $p < 0.05$ and that were in a contiguous cluster of at least three electrodes. The central prefrontal cortex (cPFC) and right primary motor cortex (rM1) regions of interest from previous analyses are highlighted with green hexagons. The functional connectivity metric used was weighted phase lag index (wPLI).

shift in peak frequency towards lower frequency (~4 Hz) with nested rules compared to higher frequency (~7 Hz) with direct mapping of stimulus to action (Senoussi et al., 2020). The authors restricted their analysis a priori to the 4–7 Hz window, thus, precluding the discovery of a potential 2–3 Hz peak as found in our analyses. Nonetheless, the similarity in cognitive control manipulations and time-frequency results provide supplementary evidence that the distinction between delta and theta oscillations captures behaviorally relevant neural variance.

With the limited spatial resolution of EEG, future work is required to resolve the spatial origin of prefrontal control signals. We have identified three potential models to explain the distinction between delta and theta oscillations found in our experiment: (1) a flexible single control system, (2) multiplexed processes, or (3) dual systems. First, the distinction between delta and theta oscillations in prefrontal cortex may be resolved to a single system that is able to flexibly shift its peak frequency, similar to findings that the alpha oscillation shifts in peak frequency based on task demands (Samaha and Postle, 2015; Wutz et al., 2018a, 2018b). Second, delta and theta oscillations may arise from distinct neural mechanisms at the cellular scale. For example, theta oscillations are theorized to be tuned to time constants of the slow NMDA receptor variant such that neural mechanisms for synaptic plasticity are maximally engaged by volleys of neural activity that occur close to the theta rhythm (Jensen and Lisman, 1996; Huang et al., 2007). Thus, delta and theta oscillations might be tuned to different cellular mechanisms

differentially engaged by the components of cognitive control driven by task demands. Distinct frequency bands can therefore serve as labeled lines of communication that are not region specific but carry specific information within a functional network (Akam and Kullmann, 2014). Under this framework, we speculate a connection between the theta rhythm with perception-memory related plasticity (Lisman and Jensen, 2013) and the delta rhythm with predictions errors in learning (Arnal et al., 2014; Cavanagh, 2015).

Third, delta and theta oscillations may be resolved as signals corresponding to two distinct systems in prefrontal cortex. In the dual systems model, theta and delta oscillations are resolved to distinct subregions of prefrontal cortex and mediate connectivity with two functionally distinct networks of brain regions. The dual systems might be medial prefrontal cortex in the default mode network and lateral prefrontal cortex in the executive control network (Yeo et al., 2011) such that theta oscillations originating in medial prefrontal cortex might reflect memory access via functional connectivity with hippocampus (Backus et al., 2016) whereas delta oscillations from the lateral prefrontal cortex might reflect motor control via functional connectivity with dorsal striatum (Antzoulatos and Miller, 2014) (see (Freedberg et al., 2020) for a review of competition between these networks). Alternatively, the dual systems might resolve to theta oscillations in the dorsal premotor area of the dorsal attention network and delta oscillations in the anterior middle frontal gyrus of the executive control network, similar to the networks found in a functional magnetic resonance imaging (fMRI) study that manipulated task abstraction (Nee and Brown, 2012). Finally, the dual systems might corresponds to two memory networks (Ranganath and Ritchey, 2012) based on recent work that dissociated low-frequency oscillations in distinct subregions of the hippocampus in human electrocorticography: posterior hippocampus was around 8 Hz (theta) and anterior hippocampus was around 3 Hz (delta) (Goyal et al., 2020). Concurrent EEG and fMRI is required to resolve which of the proposed dual systems, if any, is associated with delta and theta oscillations: frontal-parietal versus default mode, dorsal attention versus executive control, or anterior versus posterior hippocampal network.

As with any scientific study, the work presented here has limitations. The present study did not utilize methodologies with high spatial resolution. Thus, this study would need to be completed with concurrent fMRI to resolve between the provided hypotheses for a spatial origin to the delta-theta distinction. In addition, while we found general evidence that beta oscillations were concentrated in motor electrodes and gamma oscillations were concentrated in more visually selective electrodes, there is insufficient spatial resolution to make a strong assertion that the observed cross-frequency coupling patterns were indeed specific to prefrontal, motor, and parietal-occipital cortices. Furthermore, EEG signal was corrupted by artefacts during stimulation and, thus, we could not analyze entrainment from CF-tACS directly. In addition, the flexibility of tACS to target a wide-variety of specific spatial and temporal patterns of neural activity should provoke future research that investigates the relative importance of various montage decisions. Despite this inherent complexity, the double-dissociation presented here for distinct cross-frequency coupling motifs in components of cognitive control provides a foundation for additional optimization.

Future studies could be conducted to investigate the relative contributions of low-frequency stimulation versus cross-frequency stimulation. However, a previous investigation that utilized cross-frequency tACS surveyed a variety of stimulation waveforms across three experiments (Alekseichuk et al., 2016). These authors found that while the low-frequency component, theta-frequency in their experiment, alone produced an improvement in the targeted behavioral outcome, cross-frequency coupled, theta-gamma, stimulation produced an effect size with a greater magnitude. On the contrary, the high-frequency component on its own was insufficient to produce a behavioral effect. In our interpretation, the finding of this study justifies the investigation of the cross-frequency waveforms without concurrent investigation of the individual components of the stimulation waveform. Our findings assert a causal role for phase-amplitude coupling in components of cognitive control, but conclusions should not be drawn about each oscillation in isolation. Nonetheless, we speculate based on this previous experiment that the low-frequency component (delta or theta stimulation) would produce similar but weaker effects to the cross-frequency waveform.

In our preregistration, delta-beta tACS was hypothesized to improve performance as a function of abstraction. While we found that behavior was modulated as a function of abstraction, and not set-size, the direction of this effect was the opposite of what was expected. We conducted several exploratory analyses to better understand this effect. First, we found that phase-amplitude coupling increased in the homologous region of motor cortex. This suggests that stimulation reconfigured the motor-control network consistent with a disruption to normal functioning. Inspired by a previous experiment that found increased functional connectivity in the low-frequency component after CF-tACS (Alekseichuk et al., 2016), we analyzed whether stimulation produced a change in delta-frequency functional connectivity with the left motor cortex. Consistent with the hypothesis that delta-beta tACS reconfigured the motor network, we found increased functional connectivity between the left motor cortex and the right motor and central prefrontal cortex for delta-beta tACS relative to sham. Thus, stimulation was specific to the targeted functional network but our desired target engagement of increasing delta-beta coupling between prefrontal and right motor cortex was not successful.

While unexpected, a potential explanation for the differential effect of theta-gamma and delta-beta stimulation may be that theta and gamma are associated with neuronal excitability (Börgers and Kopell, 2008; Bastos et al., 2018; Bosman et al., 2012), whereas beta is general associated with neuronal inhibition (Bastos et al., 2018; Prokic et al., 2015; Rossiter et al., 2014). When stimulation is targeted to a frequency band that is inhibitory, the brain may respond with reconfiguration. For example, major depressive disorder is associated with elevated inhibitory alpha oscillations in left prefrontal cortex, yet early treatment paradigm stimulated left frontal cortex in alpha frequency (Fitzgerald et al., 2009). While counterintuitive, some researchers theorized that this stimulation resulted in a homeostatic rebound by which the targeted region normalized its activity relative to the rest of the network (Leuchter et al., 2013). Future research is required to investigate whether the aftereffect of stimulation is differential when targeting excitatory versus inhibitory neural activity. We propose that to better understand delta-beta coupling within the motor-control network delta-beta tACS could be delivered during a unimanual version of the task: behavioral disruption as a function of rule abstraction may be specific to motor control over the hand contralateral to the stimulated hemisphere, or the network may be reconfigured and performance could be disrupted despite which hand is used to make a response.

Control signals in the delta and theta band might be intrinsically related to the function of beta and gamma oscillations respectively. Investigation into the role of beta and gamma oscillations has found that gamma oscillations correspond to feedforward signals while beta oscillations correspond to feedback signals based on laminar profiles (Markov et al., 2014; Bastos et al., 2015) and associated cognitive function (Fries et al., 2001; Buschman and Miller, 2007). Together, directional signaling in gamma (beta) flows from bottom-up (top-down) across the visual hierarchy in humans (Michalareas et al., 2016) and non-human primates (Bastos et al., 2015). Investigation using rhythmic transcranial magnetic stimulation provides causal evidence in support of top-down and bottom-up attention implemented in beta and gamma frequency band respectively (Riddle et al., 2019). Low-frequency activity within the delta and theta band in prefrontal cortex might extend the cognitive processes associated with beta and gamma oscillations at the local circuit level to the network level.

4. Methods

The experiment was approved by the institutional review board at the University of North Carolina at Chapel Hill and the hypotheses were preregistered on ClinicalTrials.gov (NCT03800030). 27 participants enrolled in the study and 24 completed the experiment (19 women, 5 men). Participants were ages 18–25 (mean 19.7, sd 1.55), right-handed, normal to corrected vision, and not colorblind. Participants were excluded with neurological or medical diseases, personal history of mental illness, or use of mood-altering medication.

4.1. Hierarchical cognitive control task

The task used in this study was adapted from previously published studies (Badre and D'Esposito, 2007, 2009; Voytek et al., 2015a). We manipulated two components of hierarchical cognitive control, abstraction and set-size. During the response task (low abstraction conditions), participants learned the association between a colored square and a button response (Fig. 1A). The response task had two levels of set-size: a low set-size condition (in which four colored squares had to be associated with four responses) and a high set-size condition (in which eight different colored squares had to be associated with eight response options). For all conditions, participants kept their hands on the "home row" of a standard keyboard. For the low set-size condition, participants used their index and middle finger on both hands and colors were mapped onto the "d," "f," "j," and "k" keys. For the high set-size conditions, participants used the full home row with the inclusion of "a," "s," "l," and ";" and the associated ring and pinky fingers of both hands. At the start of each block, participants were informed of the complete mapping of buttons to colors and were given unlimited time to refresh their memory with the associations before beginning the block.

In the dimension task (high abstract conditions), participants were presented with a colored square that contained two objects. The color of the square indicated the dimension (shape or texture) by which the participant had to evaluate the two objects. Importantly, the high abstraction task contained two levels of set-size similar to the response task: a low set-size condition that consisted of only a single feature dimension upon which to evaluate the objects and a high set-size condition with two feature dimensions (Fig. 1B). In the high abstraction, low set-size condition, participants made a judgement along only one dimension (either texture or shape) as both of the colored squares mapped to a single dimension (e.g. a blue or purple square indicated that the participant must judge whether the two objects were the same or different in texture). In the high abstraction, high set-size condition, each of the two feature dimensions, texture and shape, was associated with two colored squares (e.g. the colors blue and purple indicated the texture dimension, the colors red and green indicated a perceptual judgement along the shape dimension). The colored squares were kept consistent across all low and high set-size blocks within a single session. For the low set-size, high abstraction conditions, participants completed one block with texture and one block with shape as the feature dimensions of interest, and the order was randomized. At the start of each block, participants were informed of which colored squares would be presented and the feature dimension with which they were associated. Participants could study the associations between color and feature dimension until they decided to start the task. In addition, participants were reminded of which finger was to be used to indicate that the objects were the "same" or "different." The pointer finger of each finger was used with its associated home-row button on the keyboard: "f" or "j." Thus, all task conditions required bimanual coordination.

In the experiment, participants performed eight blocks on each session, two of each of the four conditions. The tasks blocks were randomized such that the first four and last four blocks contained all conditions and the same condition of task block was never performed twice in a row. Each block contained 48 trials; thus, each participant completed 96 trials per experimental condition per session. Each trial was presented on the screen for two seconds and participants were instructed to provide their response within that time window. Each trial was separated by a fixation cross that varied exponentially in length from three to ten seconds. The experiment was programmed in Psychtoolbox implemented in MatLab 2015a (The MathWorks, Inc.). Prior to the start of the experiment on each session and after each task block, participants were instructed to maintain their gaze on a fixation point, to remain still, and to stay awake for two minutes with eyes open. The resting-state period was recorded to analyze the after-effects of stimulation.

For every session, the rules were randomized such that participants had to learn new associations. During the practice period for every session, participants were required to score at least 70% before moving onto the next practice block. These task manipulations reduced learning effects across the four experimental sessions, but help to ensure that participants learned the new task rules before beginning stimulation and EEG recording. Despite these precautions, one participant passed the practice sessions and baseline session with normal performance levels, then proceeded to respond at chance during all stimulation sessions. This participant was removed from all analyses. Thus, the final analysis comprised data from 23 participants. In addition, for one block of the high abstraction and low set-size condition, a single participant confused the texture for shape rule. In that one block, the responses for that participant were inverted such that her performance of 0% (note that chance performance is 50%) to 100% accuracy and was included in the analysis.

4.2. Cross-frequency transcranial alternating current stimulation

The stimulation montage and waveform of cross-frequency transcranial alternating current stimulation (CF-tACS) was designed to maximally target endogenous phase-amplitude coupling between the right lateral prefrontal cortex and the motor cortex / lateral parietal cortex. Prior to the start of the experiment, the electric field distribution was calculated by the tES LAB 1.0 software (Neurophet Inc., Seoul, South Korea). The montage that was selected consisted of two stimulation-pads over the right prefrontal cortex and over the right motor cortex (Fig. 4C). These two target sites received in-phase stimulation from two Neuroconn DC Plus stimulators (Neuroconn Ltd., Ilmenau, Germany). In most task-based contrasts of baseline versus all task conditions activity, there is increased activation of the medial prefrontal cortex reflecting the standard pattern of default mode activity (Raichle, 2010). Thus, the return site, connected by a split wire to both stimulators, was selected to be over the medial prefrontal cortex and received stimulation anti-phase to the target sites. As anti-phase stimulation is an inevitability of tACS designs (see (Polanía et al., 2012)), we decided that targeting the task-negative medial prefrontal cortex anti-phase to stimulation to task-positive lateral prefrontal cortex most closely approximated endogenous activity.

Three silicone-carbon electrodes, referred to as "stimulation-pads" to reduce confusion with EEG electrodes, were attached to the scalp using electrically conductive paste (Ten20, Bio-Medical Instruments, Clinton Township, MI, USA). The placement of each stimulation-pad was aligned using the International 10–20 measurement system (Klem et al., 1999). After mapping out C4, F4, Cz, and Fz on the scalp, the return stimulation-pad (5 by 7 cm) was placed at the midpoint between Fz and Cz and oriented in an anterior to posterior direction with the lead exiting posterior. Next, the first target stimulation-pad (4.5 by 4.5 cm) was placed with one corner touching the F4 location such that it was anterior and ventral to F4 with the lead exiting posterior. Finally, the second target stimulation-pad (4.5 by 4.5 cm) was placed along the central axis (C4 to Cz to C3) such that the distance to the FCz stimulation-pad was roughly equidistant to the distance between the FCz and F4 stimulation-pads. Prior to stimulation, the impedance of each stimulation-pad pair (F4 and FCz; C4 and FCz) was ensured to be below 10 kΩ. Stimulation was delivered via the "remote in" function and was

controlled by a digital-analog converter (National Instruments, Austin, TX, USA) run in the background environment via MatLab.

The remote-in feature converts a digital signal of arbitrary shape into current. The stimulation waveform for this experiment consisted of a low-frequency component delivered at 0.6 mA (1.2 mA peak-to-peak) delivered in a constant sine wave and a high-frequency component, 3.5 cycles of a sine wave delivered at 0.4 mA (0.8 mA peak-to-peak), that was superimposed on the low-frequency component and centered on the peak of each cycle. We chose to use 3.5 cycles of the high-frequency component to prevent sharp current transitions. The current for the slow (0.6 mA) and fast component (0.4 mA) were chosen such that the input current of the superimposed waveform to the target stimulation-pads did not exceed 1 mA (2 mA peak-to-peak), and the return stimulation-pad did not exceed 2 mA (4 mA peak-to-peak). For all conditions, the stimulation slowly ramped up over the course of 12 s, then the task began soon after maximum stimulation output was reached. Stimulation was maintained at a stable level until the task was complete and the stimulation ramped down over 12 s. Previous literature reports that participants are sensitive to stimulation until the sensory neurons in the skin acclimate to the stimulation. Thus, in our instructions to participants we explain that one session is a placebo, but also inform them that they will acclimate to the stimulation soon after it begins. As an active control condition, sham stimulation was delivered. For sham, a genuine cross-frequency waveform was delivered for 12 s at maximum strength and then ramp-down was initiated. The ramp-up and ramp-down during the sham stimulation was designed to mimic the feeling of acclimation that is often experienced with verum stimulation.

The sequence of three stimulation conditions was counter-balanced and randomized. A custom script generated arbitrary six-digit codes for each participant. The mapping from six-digit code to stimulation waveform was kept in a binary file that was not able to be opened via user-friendly applications. The mapping from stimulation code to stimulation waveform was maintained by another member of the lab to ensure that research personnel could not recover which stimulation waveform was delivered. At the completion of each stimulation session, both the participant and research personnel guessed whether or not verum stimulation was delivered. For delta-beta CF-tACS, 62.5% of participants believed that verum stimulation was delivered, and experimenters guessed that 70.8% of these sessions involved verum stimulation. For theta-gamma CF-tACS, 62.5% of participants believed that verum stimulation was delivered, and experimenters guessed that 54.2% of these sessions involved verum stimulation. For sham CF-tACS, 62.5% of participants believed that verum stimulation was delivered, and experimenters guessed that 58.3% of these sessions involved verum stimulation. Thus, we found exactly 0% difference in reported belief for conditions with verum stimulation versus sham stimulation suggesting that participants were blind to the form of stimulation delivered. In sessions with theta-gamma CF-tACS, the experimenters reported a greater belief that sham stimulation was delivered compared to the sham stimulation sessions, whereas delta-beta CF-tACS showed marginally less belief that sham stimulation was delivered. These fluctuations in experimenter belief are expected from a random decision process with an assumed probability of 66.67%. Altogether, these data provide evidence that the experiment was successfully double-blinded.

Side effects of stimulation were monitored and participants were informed that they could terminate the experiment at any time. Upon completion of each stimulation session, participants completed a side effects questionnaire. An adverse event was defined as any side effect reported by participants. All side effects were deemed mild and expected. The percentage of participants that experienced each side effect is reported in Table S1. This table can also be found on ClinicalTrials.gov (NCT03800030).

4.3. EEG preprocessing

EEG data were collected with a high-density 128-channel electrode net at 1000 Hz (HydroCel Geodesic Sensor Net) and EGI system (NetAmps 410, Magstim Electrical Geodesics Inc., OR, USA). The impedance of each electrode was below 50 kΩ at the start of each session. For the sessions with tACS, three conductive stimulation-pads were applied on the scalp. EEG electrodes that were at the border surrounding the stimulation-pad were not filled with gel. If they were, then this would increase the surface over which stimulation was applied to the region. Thus, some electrodes did not contain any neural signal and were interpolated early in the preprocessing pipeline (see below). In addition, EEG electrodes that were directly over a stimulation pad were filled with gel and applied. The stimulation-pads were electrically conductive and neural signal could be recorded from these electrodes. However, EEG electrodes over the same stimulation pad were bridged and thus recorded the same signal. Furthermore, the Cz electrode served as the reference electrode in the EGI system. With the return stimulation-pad centered on FCz the posterior edge extended near to the Cz EEG electrode. Experimenters ensured that the Cz electrode was not touching the return stimulation-pad and that dry scalp separated the two.

Data were preprocessed using the EEGLAB toolbox (Delorme and Makeig, 2004) in MATLAB. The preprocessing pipeline for the resting-state data was identical to the task data with the following noted exceptions. First, data from all eight task blocks was extracted and concatenated. We applied a high pass filter of 1 Hz and a low pass filter at 59 Hz. Thus, 59 Hz set the upper boundary for analysis of gamma frequency activity (35−59 Hz). Data were downsampled from 1000 Hz to 200 Hz. The data were then cleaned using an artifact subspace reconstruction algorithm to remove high-variance signal and reconstruct missing data (Mullen et al., 2013). This algorithm also flagged noisy channels which were then replaced with a spherical interpolation from its neighboring channels. Global average re-referencing was applied, which is an approximate solution for the spherical electrical field assumption that was enabled by use of a 128-channel system that includes electrode coverage on the cheeks. Data from 1 s prior and 2 s after presentation of the stimulus were extracted. Data were baseline corrected to the average of -1 s to -0.3 s relative to stimulus onset. Principal component analysis was run based on the rank of the data matrix to optimize the data for artifact rejection using info-max independent component analysis. All independent components were visually inspected and components that corresponded to line noise, muscle activity, eye movement, blinks, and heart beat were removed from the data.

The preprocessing pipeline for the resting-state data was identical to task with the following noted exceptions. Data was concatenated for all nine resting-state periods. First, data were filtered and downsampled. Then, the data were cut into two second epochs and visually inspected. Epochs with excess noise were removed, and noisy electrodes were interpolated. Next artifact subspace reconstruction, global average rereferencing, and independent component analysis with component rejection were run.

4.4. Spectral analysis

Data was extracted locked to the onset of the decision period and baseline corrected from -600 to -300 milliseconds. Five-cycle Morlet wavelets were convolved with the decision epoch for 2–58 Hz in an adjusted log distribution, with 150 frequencies evenly spaced according to Eq. (1) in order to approximate the naturally-occurring power distribution of human brain activity.

$$pwr = {}^{1}/_{freq^{0.05}} \quad (1)$$

The exponent of 0.05 was selected based on a typical recording in healthy adults using a similar method (Voytek et al., 2015b). EEG data were mirrored prior to wavelet convolution to reduce edge artifacts, then the trial averaged data for each condition was baseline corrected in time-frequency domain to -600 to -300 milliseconds from the decision

epoch. Phase-amplitude coupling was calculated using the phase and amplitude values derived from five-cycle Morlet wavelet convolution on the mirrored timeseries for exhaustive comodulograms of all frequency pairs and from Hilbert transform of band-filtered data for topographic analysis. For each participant, the phase (θ, lower frequency oscillation) and amplitude (M, higher frequency oscillation) values of each trial for the time window of interest were concatenated into a single continuous time series (n is the number of time points) and phase-amplitude coupling (PAC) was calculated according to Eq. (2) (Cohen, 2014).

$$PAC = \left| \frac{\sum_{t=1}^{n} M * e^{i\theta}}{n} \right| \quad (2)$$

PAC values were permutation corrected by temporally shifting the amplitude values with a random temporal offset of at least 10 % the length of the time series and calculating PAC (Cohen, 2014). After 1000 repetitions, PAC was converted to a z-score from the null distribution, resulting in PAC_Z.

Frequency localization was run using an exhaustive comodulogram of frequencies 2–8 Hertz in increments of 0.25 and from 9 to 59 Hz in increments of 0.25. The peak PAC_Z value between 2−4 Hz phase and 18−30 Hz amplitude and between 4−7.5 Hz phase and 35−59 Hz amplitude was calculated for all conditions. The peak value was compared against the plot of the comodulogram to ensure that the peak value was within a cluster of increased PAC values and was not spurious. For delta-beta, the high abstraction and high set-size condition was used for localization. For theta-gamma, the low abstraction and high set-size condition was used for localization. These conditions showed the greatest coupling within these bands in our previous study (Riddle et al., 2020). If a peak coupling strength could not be localized due to low or spurious PAC in the comodulogram, then canonical stimulation frequencies were chosen: 2 with 20 Hz and 5 with 50 Hz.

Weighted phase lag index (wPLI) was used to estimate frequency-specific functional connectivity, because wPLI quantifies the degree to which two signals have a consistent non-zero phase lag and this accounts for the confound of zero-lag phase lag connectivity that arises from volume conduction in EEG (Vinck et al., 2011) (Eq. (3)).

$$wPLI = \left| \sum_{t=1}^{N} \mathrm{imag}\left(\mathscr{H}(A) * \overline{\mathscr{H}(B)} \right) \Big/ N \right| \quad (3)$$

$\mathscr{H}$ is Hilbert transform, *imag* takes the imaginary component, *t* is time, *N* is number of time point. *A* and *B* are signals.

After band-filtering, the Hilbert transform extracted the instantaneous phase and amplitude of two signals. Then, the cross-spectral density of those signal is calculated for every time point. The cross-spectral density is the product of the analytic signal of one signal with the complex conjugate of the analytic signal of the other signal. Then, the imaginary component of the result is averaged over all time points and the magnitude of the resulting vector is the degree of functional connectivity (wPLI).

4.5. Statistical analysis

Behavior at baseline was investigated using repeated-measures analysis of variance (ANOVA) using two factors: abstraction (high and low) and set-size (high and low). We hypothesized that performance would be worse (lower accuracy and greater response time) as a function of set-size, but less so as a function of abstraction. To investigate the impact of CF-tACS on behavior, we ran an analysis of covariance (ANCOVA) using three-factors of interest and a control factor. The control factor (sequence) was run as a linear variable to estimate any changes to performance over sessions, such as any practice effects that may accumulate with time. The three-factors of interest were stimulation condition (delta-beta, theta-gamma, or sham), abstraction (high or low), and set-size (high or low). Following a significant main effect or interaction with the stimulation factor, post-hoc t-tests were used to determine which conditions were driving the effects. We hypothesized that delta-beta stimulation would modulate performance as a function of abstraction, but not set-size; and theta-gamma stimulation would modulate performance as a function of set-size, but not abstraction. These hypotheses were pre-registered on ClinicalTrials.gov (NCT03800030).

To investigate the distinction between delta and theta oscillations as a function of cognitive control component, we used two approaches. The first approach mirrored that of our previous study. The time-frequency data for each participant was analyzed using a pair-wise *t*-test for each time-frequency pixel. Then, the t-statistics from this test were submitted to a permutation-based cluster analysis where the label as "high" or "low" was flipped for a randomly chosen half of the participants. For each randomly labeled map of t-statistics a threshold at $p < 0.05$ was applied and the maximum average t-statistic within each cluster greater than 30 was stored, referred to as the mass. The random permutation and maximum mass calculation was performed 1000 times. The null distribution of mass values was sorted from minimum to maximum, and the 25th and 975th value were used as the significance threshold ($p < 0.05$). The second approach was to quantify a priori the amplitude of delta (2−3 Hz) and theta (4−7 Hz) oscillations from 0.2 to 1.6 s after the presentation of the stimulus in anterior prefrontal electrodes. These amplitude values were submitted to a two-way repeated-measures ANOVA with factors: low frequency band (delta or theta) and cognitive control component (abstraction contrast or set-size contrast).

To quantify the efficacy of CF-tACS to boost endogenous phase-amplitude coupling (PAC), a staged analysis was employed to reduce multiple comparisons. First, peak delta and theta oscillations were localized across the scalp as a function of abstraction and set-size. Second, this region of interest was used as a seed for the phase of low-frequency oscillations to the amplitude of high-frequency oscillations across the scalp. Seed-based PAC was calculated for all task conditions and the difference between high and low cognitive control component was calculated. Delta-beta PAC was investigated as a function of abstraction and theta-gamma was investigated as a function of set-size. Significance was set at $p < 0.05$ with at least 4 contiguous or homologous electrodes. Regions of interest were drawn around significant electrodes and then submitted to a final analysis of the impact of CF-tACS on coupling strength. We hypothesized that delta-beta CF-tACS would increase delta-beta PAC and theta-gamma CF-tACS would increase theta-gamma PAC. Thus, a two-way repeated-measured ANCOVA with one control factor was run. The factors of interest were the stimulation frequency-pair (delta-beta, theta-gamma, or sham) and the measured frequency-pair (delta-beta or theta-gamma). A linear control factor for sequence was included to account for any non-specific effects of experiment participation over time. We hypothesized an interaction between the stimulation frequency-pair and the measured frequency-pair. In addition, we hypothesized an increase in the targeted frequency band. Thus, a single *t*-test was used to evaluate the hypothesized interaction. First, phase-amplitude coupling during sham tACS was subtracted from target stimulation. Then, the interaction was defined as delta-beta PAC for delta-beta tACS versus theta-gamma tACS plus theta-gamma PAC for theta-gamma tACS versus delta-beta tACS. Given the strong a priori hypothesis and the fact that phase-amplitude coupling cannot be negative, a one-sided pair-wise *t*-test was used to evaluate the hypothesized interaction for successful target engagement.

As an exploratory analysis to understand the topological spread of stimulation effects, we also analyzed the strength of phase-amplitude coupling during post-stimulation resting-state using the seeds established at baseline. A two-tailed *t*-test was run versus zero and a cluster threshold of at least three contiguous electrodes was applied. We hypothesized that stimulation effects would be stronger in the stimulated hemisphere.

As a follow-up exploratory analysis, we investigated whether the

unexpected pattern of phase-amplitude coupling effects for delta-beta tACS coincided with an increase in functional connectivity among the motor-control network, defined as bilateral motor cortex and central prefrontal cortex. Based on a previous study that found that CF-tACS increased functional connectivity within the low-frequency component, we investigated whether delta-frequency (2−3 Hz) functional connectivity increased after delta-beta tACS relative to sham. Functional connectivity was calculated with a seed in the C3 electrode to the rest of the scalp, except electrodes surrounding C3 and electrodes surrounding those electrodes were removed from analysis as these local electrodes exceed the spatial resolution of EEG. Functional connectivity (wPLI; see Eq. (3)) was calculated for each two-minute resting-state period after each stimulation block and the resulting value was averaged across post-stimulation periods for each session. To investigate the change in delta-frequency functional connectivity with stimulation within the motor-control network, the values for FCz and surrounding and C4 and surrounding were averaged. Then, the difference between delta-beta tACS and sham was tested with a pair-wise Student's *t*-test with the hypothesis that functional connectivity would be greater for delta-beta tACS relative to sham. As a control analysis, we hypothesized no difference in functional connectivity for theta-gamma tACS versus sham. To understand the spatial specificity of these effects, a pair-wise *t*-test was run for all scalp electrodes for delta-beta tACS and theta-gamma tACS (versus sham) with a threshold of $p < 0.05$ and a cluster threshold of at least three contiguous electrodes.

Declaration of Competing Interest

The authors report no declarations of interest.

Acknowledgements

This study was supported in part by the National Institute of Mental Health of the National Institutes of Health under Award Numbers R01MH101547 and R01MH111889 awarded to FF and the postdoctoral training program T32MH09331502 (JR). The project described was supported by the National Center for Advancing Translational Sciences (NCATS), National Institutes of Health, through Grant Award Number UL1TR001111. The content is solely the responsibility of the authors and does not necessarily represent the official views of the NIH. The authors thank Alexandra Reardon and Emma Milligan for help with data collection.

FF is the lead inventor of IP filed by UNC. FF is founder, shareholder, and chief science officer of Pulvinar Neuro, which did not play any role in the writing of this article. FF has received honoraria from the following entities in the last twelve months: Sage Therapeutics, Academic Press, Insel Spital, and Strategic Innovation.

Appendix A. The Peer Review Overview and Supplementary data

The Peer Review Overview and Supplementary data associated with this article can be found in the online version, at doi:https://doi.org/10.1016/j.pneurobio.2021.102033.

References

Ahn, Sangtae, Mellin, Juliann M., Alagapan, Sankaraleengam, Alexander, Morgan L., Gilmore, John H., Fredrik Jarskog, L., Fröhlich, Flavio, 2019. 'Targeting reduced neural oscillations in patients with schizophrenia by transcranial alternating current stimulation'. NeuroImage 186, 126–136.

Akam, Thomas, Kullmann, Dimitri M., 2014. Oscillatory multiplexing of population codes for selective communication in the mammalian brain. Nat. Rev. Neurosci. 15, 111–122.

Alekseichuk, Ivan, Turi, Zsolt, Amador de Lara, Gabriel, Antal, Andrea, Paulus, Walter, 2016. 'SPatial working memory in humans depends on theta and high gamma synchronization in the prefrontal cortex'. Curr. Biol. 26, 1513–1521.

Ali, Mohsin M., Sellers, Kristin K., Fröhlich, Flavio, 2013. 'Transcranial alternating current stimulation modulates large-scale cortical network activity by network resonance'. J. Neurosci. 33, 11262–11275.

Antzoulatos, Evan G., Miller, Earl K., 2014. 'Increases in functional connectivity between prefrontal cortex and striatum during category learning'. Neuron 83, 216–225.

Antzoulatos, Evan G., Miller, Earl K., 2016. 'SYnchronous beta rhythms of frontoparietal networks support only behaviorally relevant representations'. Elife 5, e17822.

Arnal, Luc H., Doelling, Keith B., Poeppel, David, 2014. 'DElta–beta coupled oscillations underlie temporal prediction accuracy'. Cereb. Cortex 25, 3077–3085.

Backus, Alexander R., Schoffelen, Jan-Mathijs, Szebényi, Szabolcs, Hanslmayr, Simon, Doeller, Christian F., 2016. 'Hippocampal-prefrontal theta oscillations support memory integration'. Curr. Biol. 26, 450–457.

Badre, David, D'Esposito, Mark, 2007. 'Functional magnetic resonance imaging evidence for a hierarchical organization of the prefrontal cortex'. J. Cogn. Neurosci. 19, 2082–2099.

Badre, David, D'Esposito, Mark, 2009. 'Is the rostro-caudal axis of the frontal lobe hierarchical?'. Nat. Rev. Neurosci. 10, 659.

Badre, David, Nee, Derek Evan, 2018. 'Frontal cortex and the hierarchical control of behavior'. Trends Cogn. Sci. 22, 170–188.

Bastos, Andre Moraes, Vezoli, Julien, Bosman, Conrado Arturo, Schoffelen, Jan-Mathijs, Oostenveld, Robert, Dowdall, Jarrod Robert, De Weerd, Peter, Kennedy, Henry, Fries, Pascal, 2015. 'Visual areas exert feedforward and feedback influences through distinct frequency channels'. Neuron 85, 390–401.

Bastos, André M., Loonis, Roman, Kornblith, Simon, Lundqvist, Mikael, Miller, Earl K., 2018. Laminar recordings in frontal cortex suggest distinct layers for maintenance and control of working memory. Proc. Natl. Acad. Sci. 115, 1117–1122.

Berger, B., Griesmayr, B., Minarik, T., Biel, A.L., Pinal, D., Sterr, A., Sauseng, P., 2019. 'Dynamic regulation of interregional cortical communication by slow brain oscillations during working memory'. Nat. Commun. 10.

Börgers, Christoph, Kopell, Nancy J., 2008. 'Gamma oscillations and stimulus selection'. Neural Comput. 20, 383–414.

Bosman, Conrado A., Schoffelen, Jan-Mathijs, Brunet, Nicolas, Oostenveld, Robert, Bastos, Andre M., Womelsdorf, Thilo, Rubehn, Birthe, Stieglitz, Thomas, De Weerd, Peter, Fries, Pascal, 2012. 'Attentional stimulus selection through selective synchronization between monkey visual areas'. Neuron 75, 875–888.

Bramson, Bob, den Ouden, Hanneke E.M., Toni, Ivan, Roelofs, Karin, 2020. Improving emotional-action control by targeting long-range phase-amplitude neuronal coupling. Elife 9, e59600.

Braver, Todd S., 2012. The variable nature of cognitive control: a dual mechanisms framework. Trends Cogn. Sci. 16, 106–113.

Buschman, Timothy J., Miller, Earl K., 2007. Top-down versus bottom-up control of attention in the prefrontal and posterior parietal cortices. Science 315, 1860–1862.

Buschman, Timothy J., Denovellis, Eric L., Diogo, Cinira, Bullock, Daniel, Miller, Earl K., 2012. Synchronous oscillatory neural ensembles for rules in the prefrontal cortex. Neuron 76, 838–846.

Canolty, Ryan T., Knight, Robert T., 2010. The functional role of cross-frequency coupling. Trends Cogn. Sci. 14, 506–515.

Cavanagh, James F., 2015. Cortical delta activity reflects reward prediction error and related behavioral adjustments, but at different times. NeuroImage 110, 205–216.

Cohen, Mike X., 2014. Analyzing Neural Time Series Data: Theory and Practice. MIT press.

de Lara, Gabriel Amador, Alekseichuk, Ivan, Turi, Zsolt, Lehr, Albert, Antal, Andrea, Paulus, Walter, 2018. Perturbation of theta-gamma coupling at the temporal lobe hinders verbal declarative memory. Brain Stimul. 11, 509–517.

de Vries, Ingmar E.J., van Driel, Joram, Karacaoglu, Merve, Olivers, Christian N.L., 2018. Priority switches in visual working memory are supported by frontal delta and posterior alpha interactions. Cereb. Cortex 28, 4090–4104.

Delorme, Arnaud, Makeig, Scott, 2004. EEGLAB: an open source toolbox for analysis of single-trial EEG dynamics including independent component analysis. J. Neurosci. Methods 134, 9–21.

Fitzgerald, Paul B., Hoy, Kate, McQueen, Susan, Maller, Jerome J., Herring, Sally, Segrave, Rebecca, Bailey, Michael, Been, Greg, Kulkarni, Jayashri, Daskalakis, Zafiris J., 2009. 'A randomized trial of rTMS targeted with MRI based neuro-navigation in treatment-resistant depression'. Neuropsychopharmacology 34, 1255–1262.

Freedberg, Michael, Toader, Andrew C., Wassermann, Eric M., Voss, Joel L., 2020. 'Competitive and cooperative interactions between medial temporal and striatal learning systems'. Neuropsychologia 136, 107257.

Fries, Pascal., 2015. 'Rhythms for cognition: communication through coherence'. Neuron 88, 220–235.

Fries, Pascal, Reynolds, John H., Rorie, Alan E., Desimone, Robert, 2001. 'Modulation of oscillatory neuronal synchronization by selective visual attention'. Science 291, 1560–1563.

Fröhlich, Flavio., 2014. 'Endogenous and exogenous electric fields as modifiers of brain activity: rational design of noninvasive brain stimulation with transcranial alternating current stimulation'. Dialogues Clin. Neurosci. 16, 93.

Fröhlich, Flavio, McCormick, David A., 2010. 'Endogenous electric fields may guide neocortical network activity'. Neuron 67, 129–143.

Gazzaley, Adam, Nobre, Anna C., 2012. 'Top-down modulation: bridging selective attention and working memory'. Trends Cogn. Sci. 16, 129–135.

Goyal, Abhinav, Miller, Jonathan, Qasim, Salman E., Watrous, Andrew J., Zhang, Honghui, Stein, Joel M., Inman, Cory S., Gross, Robert E., Willie, Jon T., Lega, Bradley, 2020. 'Functionally distinct high and low theta oscillations in the human hippocampus'. Nat. Commun. 11, 1–10.

Hermiller, Molly S., Fen Chen, Yu, Parrish, Todd B., Voss, Joel L., 2020. 'Evidence for immediate enhancement of hippocampal memory encoding by network-targeted theta-burst stimulation during concurrent fMRI'. J. Neurosci.
Huang, Ying-Zu, Chen, Rou-Shayn, Rothwell, John C., Wen, Hsin-Yi, 2007. 'The after-effect of human theta burst stimulation is NMDA receptor dependent'. Clin. Neurophysiol. 118, 1028–1032.
Jensen, Ole, Lisman, John E., 1996. 'Theta/gamma networks with slow NMDA channels learn sequences and encode episodic memory: role of NMDA channels in recall'. Learn. Mem. 3, 264–278.
Jensen, Ole, Kaiser, Jochen, Lachaux, Jean-Philippe, 2007. 'Human gamma-frequency oscillations associated with attention and memory'. Trends Neurosci. 30, 317–324.
Kastner, Sabine, Pinsk, Mark A., De Weerd, Peter, Desimone, Robert, Ungerleider, Leslie G., 1999. 'Increased activity in human visual cortex during directed attention in the absence of visual stimulation'. Neuron 22, 751–761.
Kilavik, Bjørg Elisabeth, Zaepffel, Manuel, Brovelli, Andrea, MacKay, William A., Riehle, Alexa, 2013. 'The ups and downs of beta oscillations in sensorimotor cortex'. Exp. Neurol. 245, 15–26.
Klem, G.H., Luders, H.O., Jasper, H.H., Elger, C., 1999. 'The ten-twenty electrode system of the International Federation. The International Federation of Clinical Neurophysiology'. Electroencephalogr. Clin. Neurophysiol. Suppl. 52, 3–6.
Koechlin, Etienne, Ody, Chrystele, Kouneiher, Frédérique, 2003. 'The architecture of cognitive control in the human prefrontal cortex'. Science 302, 1181–1185.
Kurmann, Rebekka, Gast, Heidemarie, Schindler, Kaspar, Fröhlich, Flavio, 2018. 'Rational design of transcranial alternating current stimulation: identification, engagement, and validation of network oscillations as treatment targets'. Clin. Transl. Neurosci. 2, 2514183X18793515.
Lee, Taraz G., D'Esposito, Mark, 2012. 'The dynamic nature of top-down signals originating from prefrontal cortex: a combined fMRI–TMS study'. J. Neurosci. 32, 15458–15466.
Leuchter, Andrew Francis, Cook, Ian A., Jin, Yi, Phillips, Bill, 2013. 'The relationship between brain oscillatory activity and therapeutic effectiveness of transcranial magnetic stimulation in the treatment of major depressive disorder'. Front. Hum. Neurosci. 7, 37.
Lisman, John E., Jensen, Ole, 2013. 'The theta-gamma neural code'. Neuron 77, 1002–1016.
Markov, Nikola T., Vezoli, Julien, Chameau, Pascal, Falchier, Arnaud, Quilodran, René, Huissoud, Cyril, Lamy, Camille, Misery, Pierre, Giroud, Pascale, Ullman, Shimon, 2014. 'Anatomy of hierarchy: feedforward and feedback pathways in macaque visual cortex'. J. Comp. Neurol. 522, 225–259.
Michalareas, Georgios, Vezoli, Julien, Van Pelt, Stan, Schoffelen, Jan-Mathijs, Kennedy, Henry, Fries, Pascal, 2016. 'Alpha-beta and gamma rhythms subserve feedback and feedforward influences among human visual cortical areas'. Neuron 89, 384–397.
Mullen, T., Kothe, C., Chi, Y.M., Ojeda, A., Kerth, T., Makeig, S., Cauwenberghs, G., Jung, T.P., 2013. Real-time modeling and 3D visualization of source dynamics and connectivity using wearable EEG. In: Conference Proceedings : … Annual International Conference of the IEEE Engineering in Medicine and Biology Society. IEEE Engineering in Medicine and Biology Society. Annual Conference, 2013, pp. 2184–2187.
Nee, Derek Evan, Brown, Joshua W., 2012. 'Rostral–caudal gradients of abstraction revealed by multi-variate pattern analysis of working memory'. NeuroImage 63, 1285–1294.
Negahbani, Ehsan, Kasten, Florian H., Herrmann, Christoph S., Fröhlich, Flavio, 2018. 'Targeting alpha-band oscillations in a cortical model with amplitude-modulated high-frequency transcranial electric stimulation'. NeuroImage 173, 3–12.
Norman, Donald A., Shallice, Tim, 1986. Attention to action. Consciousness and Self-Regulation. Springer.
Picazio, Silvia, Veniero, Domenica, Ponzo, Viviana, Caltagirone, Carlo, Gross, Joachim, Thut, Gregor, Koch, Giacomo, 2014. 'Prefrontal control over motor cortex cycles at beta frequency during movement inhibition'. Curr. Biol. 24, 2940–2945.
Polanía, Rafael, Nitsche, Michael A., Korman, Carolin, Batsikadze, Giorgi, Paulus, Walter, 2012. 'The importance of timing in segregated theta phase-coupling for cognitive performance'. Curr. Biol. 22, 1314–1318.
Prokic, Emma J., Weston, Cathryn, Yamawaki, Naoki, Hall, Stephen D., Jones, Roland S. G., Stanford, Ian M., Ladds, Graham, Woodhall, Gavin L., 2015. 'Cortical oscillatory dynamics and benzodiazepine-site modulation of tonic inhibition in fast spiking interneurons'. Neuropharmacology 95, 192–205.
Raichle, Marcus E., 2010. 'Two views of brain function'. Trends Cogn. Sci. 14, 180–190.
Ranganath, Charan, Ritchey, Maureen, 2012. 'Two cortical systems for memory-guided behaviour'. Nat. Rev. Neurosci. 13, 713–726.
Riddle, Justin, Hwang, Kai, Cellier, Dillan, Dhanani, Sofia, D'Esposito, Mark, 2019. 'Causal evidence for the role of neuronal oscillations in top–Down and bottom–Up attention'. J. Cogn. Neurosci. 31, 768–779.
Riddle, Justin, Vogelsang, David A., Hwang, Kai, Cellier, Dillan, D'Esposito, Mark, 2020. 'Distinct oscillatory dynamics underlie different components of hierarchical cognitive control'. J. Neurosci. 40, 4945–4953.
Rossiter, Holly E., Davis, Emma M., Clark, Ella V., Boudrias, Marie-H.élène, Ward, Nick S., 2014. 'Beta oscillations reflect changes in motor cortex inhibition in healthy ageing'. NeuroImage 91, 360–365.
Samaha, Jason, Postle, Bradley R., 2015. 'The speed of alpha-band oscillations predicts the temporal resolution of visual perception'. Curr. Biol. 25, 2985–2990.
Schmidt, Robert, Ruiz, Maria Herrojo, Kilavik, Bjørg E., Lundqvist, Mikael, Starr, Philip A., Aron, Adam R., 2019. 'Beta Oscillations in Working Memory, Executive Control of Movement and Thought, and Sensorimotor Function'. J. Neurosci. 39, 8231–8238.
Senoussi, Mehdi, Verbeke, Pieter, Desender, Kobe, Esther De Loof, Durk Talsma, Verguts, Tom, 2020. 'Theta oscillations shift towards optimal frequency for cognitive control'. bioRxiv.
Turi, Zsolt, Mittner, Matthias, Lehr, Albert, Bürger, Hannah, Antal, Andrea, Paulus, Walter, 2020. 'θ-γ cross-frequency transcranial alternating current stimulation over the trough impairs cognitive control'. eneuro 7.
Van Kerkoerle, Timo, Self, Matthew W., Dagnino, Bruno, Gariel-Mathis, Marie-Alice, Poort, Jasper, Van Der Togt, Chris, Roelfsema, Pieter R., 2014. 'Alpha and gamma oscillations characterize feedback and feedforward processing in monkey visual cortex'. Proc. Natl. Acad. Sci. 111, 14332–14341.
Vinck, Martin, Oostenveld, Robert, Van Wingerden, Marijn, Battaglia, Franscesco, Pennartz, Cyriel M.A., 2011. 'An improved index of phase-synchronization for electrophysiological data in the presence of volume-conduction, noise and sample-size bias'. NeuroImage 55, 1548–1565.
Violante, Ines R., Li, Lucia M., Carmichael, David W., Lorenz, Romy, Leech, Robert, Hampshire, Adam, Rothwell, John C., Sharp, David J., 2017. 'Externally induced frontoparietal synchronization modulates network dynamics and enhances working memory performance'. Elife 6, e22001.
Voytek, Bradley, Canolty, Ryan T., Shestyuk, Avgusta, Crone, Nathan, Parvizi, Josef, Knight, Robert T., 2010. 'Shifts in gamma phase–amplitude coupling frequency from theta to alpha over posterior cortex during visual tasks'. Front. Hum. Neurosci. 4, 191.
Voytek, Bradley, Kayser, Andrew S., Badre, David, Fegen, David, Chang, Edward F., Crone, Nathan E., Parvizi, Josef, Knight, Robert T., D'esposito, Mark, 2015a. 'Oscillatory dynamics coordinating human frontal networks in support of goal maintenance'. Nat. Neurosci. 18, 1318.
Voytek, Bradley, Kramer, Mark A., Case, John, Lepage, Kyle Q., Tempesta, Zechari R., Knight, Robert T., Gazzaley, Adam, 2015b. 'Age-related changes in 1/f neural electrophysiological noise'. J. Neurosci. 35, 13257–13265.
Wischnewski, Miles, Joergensen, Mie L., Compen, Boukje, Schutter, Dennis J.L.G., 2020. 'Frontal Beta Transcranial alternating current stimulation improves reversal learning'. Cereb. Cortex 30, 3286–3295.
Wutz, Andreas, Loonis, Roman, Roy, Jefferson E., Donoghue, Jacob A., Miller, Earl K., 2018a. 'Different levels of category abstraction by different dynamics in different prefrontal areas'. Neuron 97, 716–726 e8.
Wutz, Andreas, Melcher, David, Samaha, Jason, 2018b. 'Frequency modulation of neural oscillations according to visual task demands'. Proc. Natl. Acad. Sci. 115, 1346–1351.
Wyart, Valentin, de Gardelle, Vincent, Scholl, Jacqueline, Summerfield, Christopher, 2012. 'Rhythmic fluctuations in evidence accumulation during decision making in the human brain'. Neuron 76, 847–858.
Yeo, B.T.Thomas, Krienen, Fenna M., Sepulcre, Jorge, Sabuncu, Mert R., Lashkari, Danial, Hollinshead, Marisa, Roffman, Joshua L., Smoller, Jordan W., Zöllei, Lilla, Polimeni, Jonathan R., 2011. 'The organization of the human cerebral cortex estimated by intrinsic functional connectivity. J. Neurophysiol.